Sub-kilometer dynamical downscaling of near-surface winds in complex terrain using WRF and MM5 mesoscale models

Kristian Horvath,[1] Darko Koracin,[2] Ramesh Vellore,[2,3] Jinhua Jiang,[2] and Radian Belu[4]

[1]   Sub-kilometer dynamical downscaling was performed using the Weather Research and Forecasting (WRF) and Mesoscale Model Version 5 (MM5) models. The models were configured with horizontal grid spacing ranging from 27 km in the outermost telescoping to 333 m in the innermost domains and verified with observations collected at four 50-m towers in west-central Nevada during July and December 2007. Moment-based and spectral verification metrics showed that the performance of WRF was superior to MM5. The modeling results were more accurate at 50 m than at 10 m AGL. Both models accurately simulated the mean near-surface wind shear; however, WRF (MM5) generally overestimated (underestimated) mean wind speeds at these levels. The dispersion errors were the dominant component of the root-mean square errors. The major weakness of WRF was the overestimation of the intensity and frequency of strong nocturnal thermally driven flows and their sub-diurnal scale variability, while the main weaknesses of MM5 were larger biases, underestimation of the frequency of stronger daytime winds in the mixed layer and underestimation of the observed spectral kinetic energy of the major energy-containing motions. Neither of the verification metrics showed systematic improvement in the models' accuracy with increasing the horizontal resolution and the share of dispersion errors increased with increased resolution. However, a profound improvement in the moment-based accuracy was found for the mean vertical wind shear and the temporal variability of wind speed, in particular for summer daytime simulations of the thermally driven flows. The most prominent spectral accuracy improvement among the primary energy-containing frequency bands was found for both models in the summertime diurnal periods. Also, the improvement for WRF (MM5) was more (less) apparent for longer-than-diurnal than for sub-diurnal periods. Finally, the study shows that at least near-kilometer horizontal grid spacing is necessary for dynamical downscaling of near-surface wind speed climate over complex terrain; however, some of the physics options might be less appropriate for grid spacing nearing the scales of the energy-containing turbulent eddies, i.e., resolutions of several hundred meters. In addition to the effects of the lower boundary, the accuracy of the lateral boundary conditions of the parent domains also controls the onset and evolution of the thermally driven flows.

1.   Introduction

[2]   The term "downscaling" refers to a methodology through which coarse gridded data, typically the results of the global reanalysis or global circulation/climate models, is refined to provide information for a regional or local interpretation. This is achieved with the use of regional and mesoscale atmospheric and climate models ('dynamical downscaling'), statistical analysis ('statistical downscaling') or a combination of both ('dynamical-statistical downscaling'). Since it has representations of physical processes, dynamical downscaling is regarded to be the most accurate approach among these methods. While computationally expensive, it has been extensively applied to the regional assessment of current and future climates using regional climate models (RCM). The reader is referred to the RCM overviews by *Giorgi* [2006] and *Intergovernmental Panel on Climate Change* [2007]. In parallel to long-term RCM

[1]Meteorological and Hydrological Service, Zagreb, Croatia.
[2]Desert Research Institute, Reno, Nevada, USA.
[3]Center for Climate Change Research, Indian Institute of Tropical Meteorology, Pune, India.
[4]School of Technology and Professional Studies, Drexel University, Philadelphia, Pennsylvania, USA.

Corresponding author: K. Horvath, Meteorological and Hydrological Service, Grič 3, 10000 Zagreb, Croatia. (kristian.horvath@cirus.dhz.hr)

applications, an increasing number of studies employ mesoscale models at grid spacing of a few kilometers for analyzing monthly or intraseasonal time scale variability in regional meteorological phenomena [e.g., *Leung et al.*, 2006; *Lo et al.*, 2008; *Caldwell et al.*, 2009; *Rife et al.*, 2010; *Trapp et al.*, 2011] and for studying or mapping of the historical near-surface wind speed climatology [*Žagar et al.*, 2006; *Jiménez et al.*, 2010; *Hahmann et al.*, 2010; *Horvath et al.*, 2011]. Therefore, with ever increasing grid refinement of regional/mesoscale weather and climate models, a rigorous assessment of dynamical downscaling at near-kilometer grid spacing is indispensable to confirm the higher-resolution modeling benefits as well as for deriving more accurate longer-term climatology estimates.

[3] The use of dynamical downscaling for the assessment of near-surface wind climatology is advantageous especially over complex terrain because atmospheric conditions resulting from the surface inhomogeneities cannot be well resolved by the global models. An increasing number of modeling studies have discussed the benefits of numerical simulations at near-kilometer grid spacing for realism of simulated winds over complex terrain regardless of the choice of a mesoscale model [e.g., *Colle and Mass*, 1998; *Zängl et al.*, 2004; *Chow et al.*, 2006; *Belušić et al.*, 2007]. Apart from showing the realism of model solutions in studies of an individual phenomenon, however, computational limitations largely constrain attempts for systematic verification of mesoscale models at near-kilometer grid spacing over a longer period of time.

[4] Verification of the mesoscale models' performance is a challenging task that seldom has been performed in a unified approach. It is often considered that the higher the resolution the more accurate the final result, due to better resolved lower boundary conditions and flow adaptation when decreasing the grid spacing. The quantitative benefits of higher resolution in mesoscale modeling and RCM research, however, are not necessarily shown by standard moment-based objective verification [*Anthes et al.*, 1989; *Mass et al.*, 2002]. For example, small errors in space and time of otherwise better simulated phenomena from a higher-resolution model often yield moment-based scores which are inferior to the scores obtained from the coarse grid model results [*Rife and Davis*, 2005]. The challenge of demonstrating the benefits quantitatively is therefore frequently studied with other scale-dependent approaches [e.g., *Feser*, 2006; *Rockel et al.*, 2008]. Nevertheless, a more meaningful moment-based analysis of the model performance could be achieved not only by verification of distributions, but also through data clustering prior to the estimation of model errors as well as by assessing the contribution of phase errors and biases of the mean and standard deviation to the RMSE [*Takacs*, 1985]. Furthermore, a complimentary spectral verification, formulated quantitatively to facilitate measurable analysis of model accuracy [*Rife et al.*, 2004], may provide spectral scale-dependent verification metrics of model performance which is tolerant of phase errors and enable qualitative physical insight into the mesoscale model results.

[5] The questions that we are aiming to address in this study are:

[6] 1. What is the accuracy of the sub-kilometer dynamical downscaling of near-surface wind speed and wind shear over complex terrain using the WRF and MM5 mesoscale models?

[7] 2. Does a uniform mesh refinement in mesoscale models uniformly enhance the accuracy of the near-surface wind speed estimates, and what is the grid spacing required for obtaining a reliable estimate of near-surface wind climate over complex terrain? How equivalent are the moment-based and spectral verification metrics in assessing the model's performance and the potential accuracy improvement with increasing the horizontal resolution?

[8] 3. What are the strengths and weaknesses of dynamical downscaling using mesoscale models and what are the rationales and/or hypothesis that can be attributed to the sources of errors?

[9] The area for dynamical downscaling conducted in this study is the complex terrain of west-central Nevada in the proximity of the Sierra Nevada and Inyo Mountain ranges in the western U.S. In our study we use two mesoscale models, the WRF and the MM5 models, which are commonly used for downscaling purposes. The models' setups include varying horizontal grid spacing ranging from 27 km in the outermost domain telescoping to 333 m in the innermost nests following a parent to nest grid ratio of 1:3. The analysis covers summer (July) and winter (December) months in 2007. Wind observations collected from the four 50-m meteorological towers were used for models' verification.

[10] This paper is organized as follows. Section 2 presents the observed aspects of wind regimes in west-central Nevada. Section 3 gives an overview of the models' setup, domains, and numerical experiments. The moment-based and spectral verification of the model results are presented in section 4, followed by the summary and conclusions in section 5.

2. Observational Analysis

[11] The area in the vicinity of the eastern slopes of the Sierra Nevada Mountains has a complex pattern of wind climate which is governed by a variety of nonlinear and non-hydrostatic phenomena. Several studies have addressed the mesoscale phenomena in this region *viz.*, diurnal flows, downslope windstorms, mesoscale cyclogenesis, and terrain-induced rotors [*Stewart et al.*, 2002; *Cairns and Corey*, 2003; *Grubišić et al.*, 2008; *Jeglum et al.*, 2010]. However, the studies relevant to terrain-induced mesoscale circulations in west-central Nevada received rather less attention.

2.1. Some Aspects of the Observed Wind Regime

[12] The focal target area in this study is located in west-central Nevada, ~100 km east of the northern tip of the Inyo Mountain Range of the Sierra Nevada Mountains (Figure 1). The region is a basin and range province, characterized by several mostly north-south oriented narrow mountain ranges. Secondary mountain ranges in the area reach elevations as high as 3000 m, and on average stand about 1500 m over the surrounding plains. The large-scale terrain tilt is greatest toward the south. The climate is generally semiarid and the vegetation is sparse. The land-cover around the stations is very uniform with isolated bushes up to 1-m height. The aridity of the region leads to a high Bowen ratio and large diurnal variations in the sensible heating in the warm part of the year. Together with the orographic features of the region,
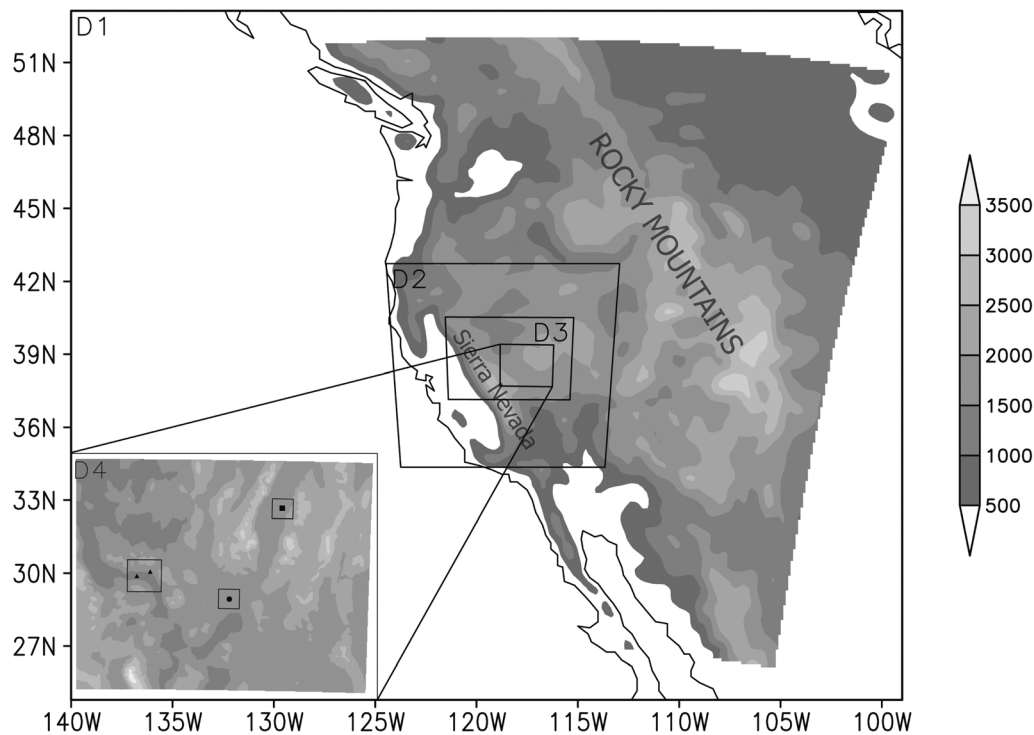
Figure 1. Model domains dmn1 (D1, grid spacing 27 km), dmn2 (D2, grid spacing 9 km), dmn3 (D3, grid spacing 3 km), dmn4 (D4, grid spacing 1 km) and three sub-kilometer domains (grid spacing 333 m) as well as the orography of the west-central Nevada and western U.S. as seen by the USGS digital elevation terrain model at 27 km grid spacing and 1 km grid spacing (inset). Locations of the wind towers are marked in the sub-kilometer domains by a closed circle (Tonopah) to the south, a closed square (Kingston) to the north and closed triangles (Luning 5N (at higher elevation) and Luning 7W (at lower elevation)) to the west.

these properties are highly conducive to the onset and maintenance of thermally driven diurnal circulations. In summer, the entire region is typically characterized by deep and extremely well-mixed daytime convective boundary layers and a strong stably stratified nocturnal boundary layer with near-surface inversions [*Whiteman*, 2000; *Stewart et al.*, 2002]. In winter, however, the atmospheric processes are mainly determined by the passages of frontal systems coming from the Pacific.

[13] The current observational network of the near-surface winds and their diurnal variability in Nevada is rather poor, except for a sparse network of surface stations and a very few field experiments. Perhaps the most extensive observational study of diurnal flows in the U.S. Intermountain West was done by *Stewart et al.* [2002] in the framework of the MesoWest network, who studied the climatology of thermally driven wind systems in the region. They suggested that besides local thermally driven circulations, regional southwesterly plain-mountain flows driven by regional-scale heating contrasts are an important component of thermally driven flows over the arid U.S. Southwest.

[14] The observed wind regime in west-central Nevada as inferred from the network of four 50-m meteorological towers (geographical locations shown in Figure 1) for the period September 2003–March 2008 was documented in *Belu and Koracin* [2009]. These towers were equipped with

RM Young 05103 four blade helicoid propeller anemometers at 10 m, 20 m, 30 m, 40 m, and 50 m above ground level (AGL). Each anemometer was individually calibrated, with accuracy within ± 0.3 ms^{-1} or 1% of the reading. At the top of the 50-m wind towers two arms with anemometers were mounted opposite to each other with azimuths of 255° and 75°. The differences in the mean wind speeds between the two sensors at the same height were on average much smaller than the sensor accuracy limit, though individually they might have occasionally reached the sensor accuracy limit individually. For example, in July 2007 the mean difference between the two sensors averaged over all towers was approximately 0.025 ms^{-1}. Therefore, the average effect of the wind towers on the data we used for analysis and verification may be considered small. The data were collected at 1 Hz frequency, quality controlled and interpolated to fill the missing data (less than 3%). For the analysis in this paper, we used data from ENE-facing sensor. More information on quality control is found in *Belu and Koracin* [2009].

[15] Two distinctly different seasonal wind regimes during summer (July 2007) and winter (December 2007) were chosen for this study. The synoptic setup over the study region during July 2007 was characterized by a strong upper-level ridge and southwesterly mean upper-level flow (Figure 2a) as inferred from the monthly composites of the
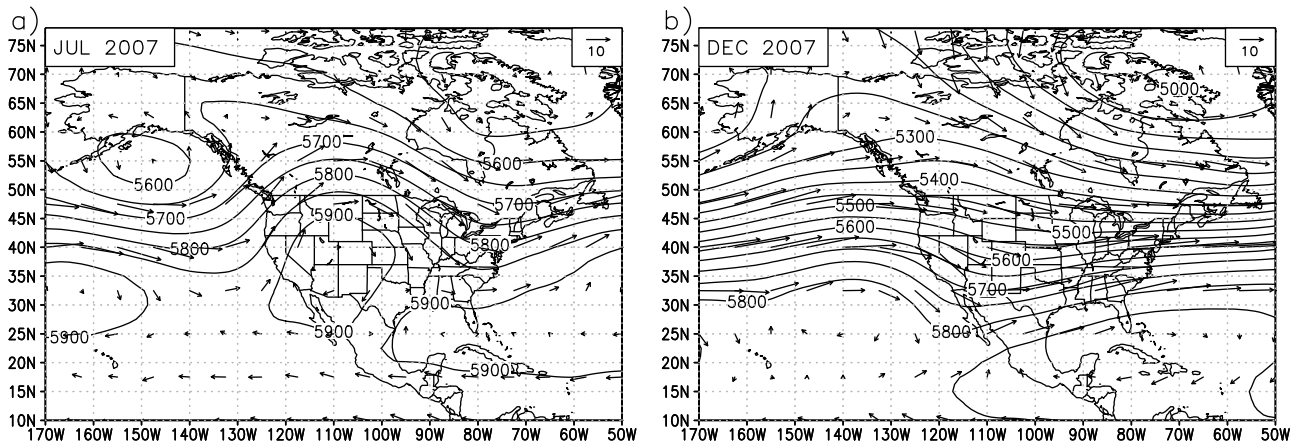
Figure 2. Composite monthly means of the geopotential height and wind vectors at 500 hPa, as inferred by the North American Regional Reanalysis (NARR) in (a) July and (b) December 2007.

North American Regional Reanalysis (NARR) [*Mesinger et al.*, 2006]. The mean upper-level low was located over the Gulf of Alaska, and troughs typically passed far north of the target area. In December 2007, however, the upper-level mean flow was nearly zonal (or WNW) resulting in occasional cyclone activity across the study region (Figure 2b).

[16] Wind rose measurements at 10 m AGL from four towers located at Tonopah (TO), Luning 5N (L5), Kingston (KI) and Luning 7W (L7) in July 2007 are shown in Figure 3. Station TO is located in nearly flat terrain, stations KI and L7 in flat-terrain valleys and station L5 on the slope near the hill-top. The width of valleys is over 20 km for KI and somewhat less for L7. The overall terrain complexity is larger in the proximity of L5 and L7 stations, than for KI and TO. The dominant flow directions at the tower TO which is located over flat terrain was SSE and at the tower L5
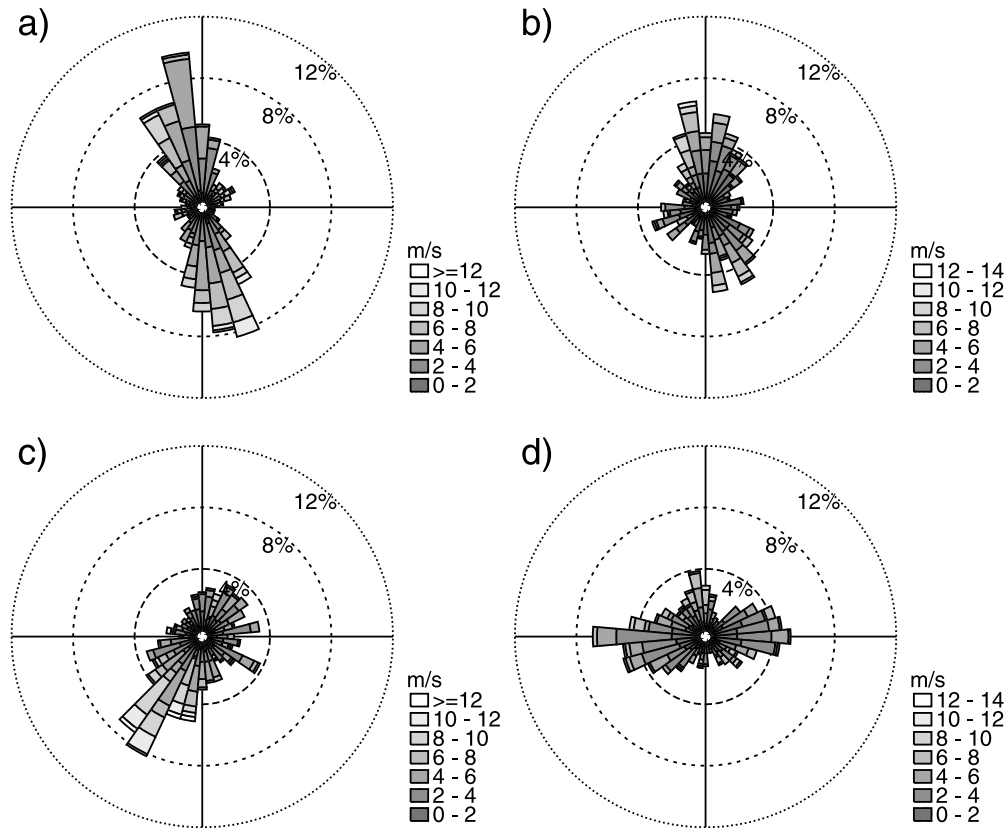

Figure 3. Wind roses at 10 m AGL for (a) Tonopah, (b) Luning 5N, (c) Kingston and (d) Luning 7W during July 2007.
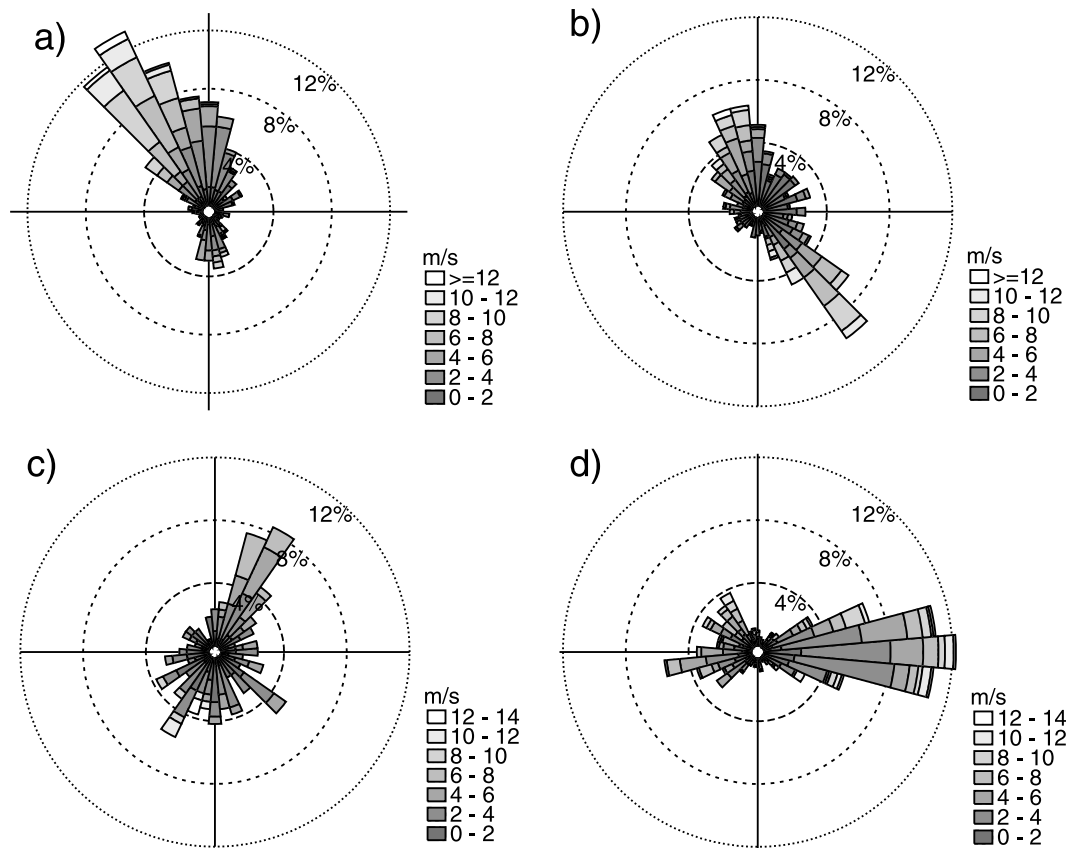
Figure 4. Wind roses at 10 m AGL for (a) Tonopah, (b) Luning 5N, (c) Kingston and (d) Luning 7W during December 2007.

which is located on the slope near the hill top was NNW. The prevailing wind directions at the KI and L7 towers, both located in valleys, were channeled to along-valley directions: SSW-NNE and W-E, respectively. The prevailing bi-polar wind direction at these locations shows topographic channeling and points to a diurnal origin of these flows. The strongest wind speeds were found at TO and KI, which also had the highest mean average wind speed during the analyzed summer month. As shown by *Belu and Koracin* [2009], the monthly mean wind speeds are generally found to be the strongest during late afternoon, and the weakest during the early morning hours.

[17] Similar prevailing wind directions are also seen in December 2007 (Figure 4). However, the setting for thermally driven flows was much less favorable in December. While the mean wind speed at TO and KI was smaller than in July 2007, the mean winds at L5 and L7 increased. The resulting wind directions for stations KI and L7 were in correspondence with the valley orientations, and the similarity of the dominant wind directions at TO and L5 (SSE-NNW) was likely related to the orientation of the Sierra Nevada and Inyo mountain ranges.

[18] The strongest monthly mean wind speeds at 10 m AGL at these stations were 6.76 at 03 UTC (19 LST) in July and 5.02 ms^{-1} 00 UTC (16 LST) in December 2007. The weakest monthly mean wind speeds at 10 m AGL were 2.3 at 14 UTC (6 LST) in July and 2.62 ms^{-1} at 11 UTC (3 LST) in December 2007. The transition between the daytime and

nighttime circulation was found to be rather abrupt with no calm transitional periods. The strongest nocturnal winds were typically found in the early hours of the night, nearly subsequent to the afternoon maxima, giving rise to strong diurnal variability of both individual wind components and wind speed values.

2.2. Spectral Analysis of Observed Wind Speed

[19] Spectral density functions are used to study the scale-dependent properties of the observed wind speed at 10 m AGL. In July 2007, the measured data from all four analyzed towers showed a pronounced peak at diurnal periods of motion (Figure 5a). The spectral density functions of the diurnal period showed amplitudes an order of magnitude higher than the individual frequencies corresponding to synoptic or longer mesoscale motions. The highest diurnal spectral density was found for the KI tower. In December 2007, the diurnal spectral peak was much weaker, an order of magnitude smaller than in July (Figure 5b). In contrast, due to common frontal passages in winter, the spectral density in the synoptic frequency range was an order of magnitude stronger in December than in July 2007.

[20] In order to assess the relative strength of circulations that have diurnal periods compared to the flows of other periods, we divided the flow regimes following *Rife et al.* [2004], into sub-diurnal (SD, 2 h < T < 22 h), diurnal (DI, 22 h < T < 26 h) and longer-than-diurnal (LTD, 26 h < T < 7 d) periods. First, the spectral density functions were calculated
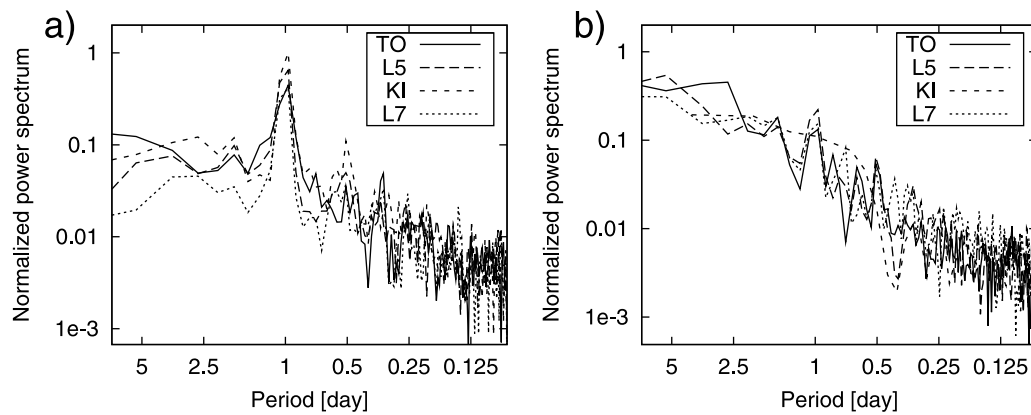
Figure 5. Spectral density functions at 10 m AGL for stations Tonopah (TO), Luning5N (L5), Kingston (KI) and Luning7W (L7) during (a) July 2007 and (b) December 2007. Data for Kingston in December 2007 were available only for the first nine days of the month.

using the *Welch* [1967] method. Second, the contribution to the wind speed variance in the chosen frequency band, i.e., the spectral kinetic energy of periodic motions associated with the chosen frequency band, was computed by integrating the spectral density functions over the given frequency range (see Appendix A for details). Although our primary aim was to isolate the strength of diurnal circulations from longer-than-diurnal and sub-diurnal motions, we note that the arbitrary selection of associated periods has a few disadvantages. First, the exact width of the diurnal band may be dependent on the technical details of the calculation, such as de-trending methods, selection of widths and overlapping of individual data segments. Second, though the wind speed had primarily diurnally varying amplitude, it is likely that a part of the energy was projected on the semi-diurnal (12 h) periods. For example, this can be seen at KI in July 2007 (Figure 5a). However, the analyzed wind characteristics in the area, especially if averaged over several stations which was our verification approach, suggested that the energy of the thermally driven flows in the region of interest was primarily contained in the diurnal range of the spectral density functions of the wind speed.

[21] The relative values of the horizontally averaged (averaged over all four towers) spectral kinetic energy in different frequency bands for July and December 2007 are shown in Table 1. In July, the contributions to the kinetic energy of all periods of motion were as follows: at 10 m AGL LTD motions contained 80%, DI motions 15% and SD motions 4%, while at 50 m AGL LTD motions contained 82%, DI motions 13% and SD motions 4%. Therefore, the strength of the LTD motions was somewhat smaller at 10 m AGL than at 50 m AGL, whereas the strength of the DI motions was somewhat larger at 10 m AGL than at 50 m AGL. This confirms that the diurnal forcing is larger closer to the ground. The spectral kinetic energy of the DI and SD motions was considerably smaller and equaled 1.5% each in December 2007 in favor of the strength of the LTD motions that reached 97%. Thus, the spectral kinetic energy of the DI and SD motions was almost negligible and almost exclusively contained in the longer-than-diurnal mesoscale and synoptic motions.

[22] To summarize, regardless of the similar bipolar wind directions, it is inferred that the underlying physical reasons for the distribution of wind directions are different. The summertime wind climate is marked by a strong component of the local and regional thermally driven diurnal circulations which develop under the quasi-stationary upper-level ridge and strong insolation contrasts. During wintertime, the energy of the diurnal flows is negligible, which confirms the dominant effect of the winter pressure systems and associated frontal passages; the origin of the bipolar wind direction is not attributed to the thermally driven circulations, but to the orientation of the primary mountain ranges in the area.

3. The Modeling Methodology

[23] The mesoscale models used in this study are Penn State/NCAR Mesoscale Model Version 5 (MM5) [*Grell et al.*, 1994], and the mass-core Advanced Research version of the Weather Research and Forecasting model (WRF) [*Skamarock et al.*, 2008]. Both are non-hydrostatic primitive equation models that have the terrain-following pressure as the vertical coordinate [see also *Laprise*, 1992]. For the temporal discretization, both models use time-splitting to maintain the numerical stability; the low frequency modes are integrated using the second-order accuracy time integration

Table 1. Horizontally Averaged Percent of Total Spectral Kinetic Energy in Different Frequency Bands in July and December 2007[a]

| | Percent of Total Spectral Kinetic Energy | | | | | |
| | July | | | December | | |
AGL	LTD	DI	SD	LTD	DI	SD
10 m	80.3	15.1	4.1	97.0	1.5	1.5
50 m	82.2	13.4	4.4	97.5	1.2	1.3

[a]Percent of total spectral kinetic energy is calculated by integrating the spectral density functions of the frequency bands corresponding to periods t > 26 h (LTD, longer-than-diurnal motions), 22 h < t < 26 h (DI, diurnal motions) and t < 22 h (SD, sub-diurnal motions). Results are horizontally averaged over all analyzed stations.

scheme for MM5 and third-order for WRF. The numerical discretization is performed on the Arakawa B-grid with a second-order horizontal advection scheme for MM5 and on the C-grid with a fifth-order horizontal advection scheme for WRF.

[24] The models were configured with seven domains; four of them having horizontal grid spacings 27 km (parent domain; referred to as 'dmn1'), 9 km ('dmn2'), 3 km ('dmn3') and 1 km ('dmn4'), respectively. Nested into the 1 km gridded domain were 3 domains (here together referred to as 'dmn5') whose horizontal grid spacing is 333 m (Figure 1). The actual size of the three sub-kilometer domains ranges from 50×50 grid points (16.7×16.7 km) to 70×70 grid points (23.3×23.3 km). The number of vertical levels was 37 with the lowest model level set at approximately 10 m AGL. The following physical parameterizations were chosen for WRF and MM5: (i) the Mellor-Yamada-Janjic scheme (1.5-order turbulence closure model) to parametrize the turbulence in the planetary boundary layer [*Mellor and Yamada*, 1974, 1982; *Janjić*, 2001] (ii) Kain-Fritsch [*Kain and Fritsch*, 1993; *Kain*, 2004] scheme (dmn1 and dmn2 only) to represent convective processes (iii) Eta surface layer scheme following Monin-Obhukov similarity theory [*Janjić*, 1996, 2001] (iv) the *Dudhia* [1989] scheme for shortwave radiation and the Rapid Radiative Transfer Model for longwave radiation [*Mlawer et al.*, 1997]. For the microphysics, the Reisner type of explicit microphysics is used in MM5 [*Reisner et al.*, 1998], while the Thompson microphysics, which is a modified version of Reisner's microphysics, is used in WRF [*Thompson et al.*, 2004]. To simulate the vertical transport of soil moisture and heat, the Noah land-surface model [*Chen and Dudhia*, 2001; *Ek et al.*, 2003] was used in WRF and a 5-layer slab model in MM5.

[25] The static lower boundary conditions, viz. topography and land use, were interpolated from the U.S. Geological Survey data sets from an arc resolution of 10′ for dmn1, 5′ for dmn2 and 30″ for all other domains. It should be mentioned that the terrain height at the tower locations differs across the domains. The largest differences are found in dmn1, where the elevations are overestimated by 272 m (TO), 446 m (KI), 192 m (L5) and 354 m (L7), or 316 m on average. The average difference is halved in dmn2 (153 m), further reduced in dmn3 (35 m) and almost nonexistent in dmn4 and dmn5 (<3 m). This overestimation of terrain height at the tower locations in the lower-resolution domains is caused by the proximity of the high and steep orography of the Inyo and Sierra Mountains to the east, and one should bear in mind that larger differences are likely to affect the model verification results.

[26] Initial and boundary conditions were provided by the three-hourly North American Regional Reanalysis (NARR) [*Mesinger et al.*, 2006]. The nesting strategy of the modeling domains was one-way, using a four-point relaxation zone. The models were initialized daily at 1200 UTC to allow for a spin-up period of 12 h in the simulation. The output data were archived with a 60-min frequency. Daily initialization, although more computationally demanding, was chosen rather than less-frequent initialization or continuous simulation for its higher accuracy [*Pan et al.*, 1999; *Qian et al.*, 2003; *Lo et al.*, 2008].

[27] It should be noted that there are a few limitations in the setup of the sub-kilometer modeling domains: (i) coarser static input data (30″ corresponding to ∼900 m) was used together with limited domain sizes, and (ii) the applicability of using planetary boundary layer parameterizations. First, the smaller domains are generally more susceptible to contamination of the results by errors associated with the lateral boundary conditions. Second, domain grid spacing of several hundred meters is the grid spacing where the scale of energy-containing turbulent eddies is close to the scale of the spatial filter, so-called "terra incognita" [*Wyngaard*, 2004]. Thus, neither the planetary boundary layer scheme, used for grid increments which do not resolve the turbulent eddies, nor the large-eddy filtering, which requires that larger turbulent eddies are resolved, are designed for use with a grid spacing of several hundred meters. The above issues might affect the models' performance in the innermost domains.

4. Results and Discussion

[28] The analysis of the model performance uses observations at 10 m and 50 m AGL from the four above mentioned wind towers. The model verification did not take into account the instrument errors, calibration errors or representativeness errors. Although the model results were interpolated to the station locations, both in horizontal and vertical directions, one should bear in mind that the comparison of the point measurements with grid values introduces inherent uncertainty over the complex terrain geometry. For example, the estimate of a representativeness error, which is the greatest among the aforementioned errors, in a model grid-box of size 1.33 km × 1.33 km is about 1 ms^{-1} for near-surface wind speed in a well-mixed boundary layer over the complex terrain [*Rife et al.*, 2004]. The representativeness error generally varies depending on the station location and decreases with height. The expected representativeness error is likely larger for towers L5 and L7, since in their very vicinity the orography is generally more complex than for towers KI and TO. While the representativeness error may be considerable in the lower-resolution domains, magnitude of the representativeness error in the sub-kilometer domains is limited due to small orography variance in the very vicinity of the four analyzed towers (e.g., in area 333 m × 333 m).

[29] The verification approach adopted in this study uses the raw model output from all domains and 10-min wind speed measurements and averages the results over all four tower locations. No additional filtering was applied to neither observed data nor model results. The analysis of verification metrics at all stations individually or according to some regionalization method could likely be beneficial for a more detailed insight into the models' performance. However, we chose to perform the averaged type of analysis since to summarize the results and due to predominantly quantitative differences among partially analyzed models' results for individual locations. In addition, the regional approach may smooth out errors introduced in the verification procedure, such as instrument accuracy, comparison of simulated wind speeds (volume averages) and point measurements, the effective time-resolution of the model data in different domains and other.
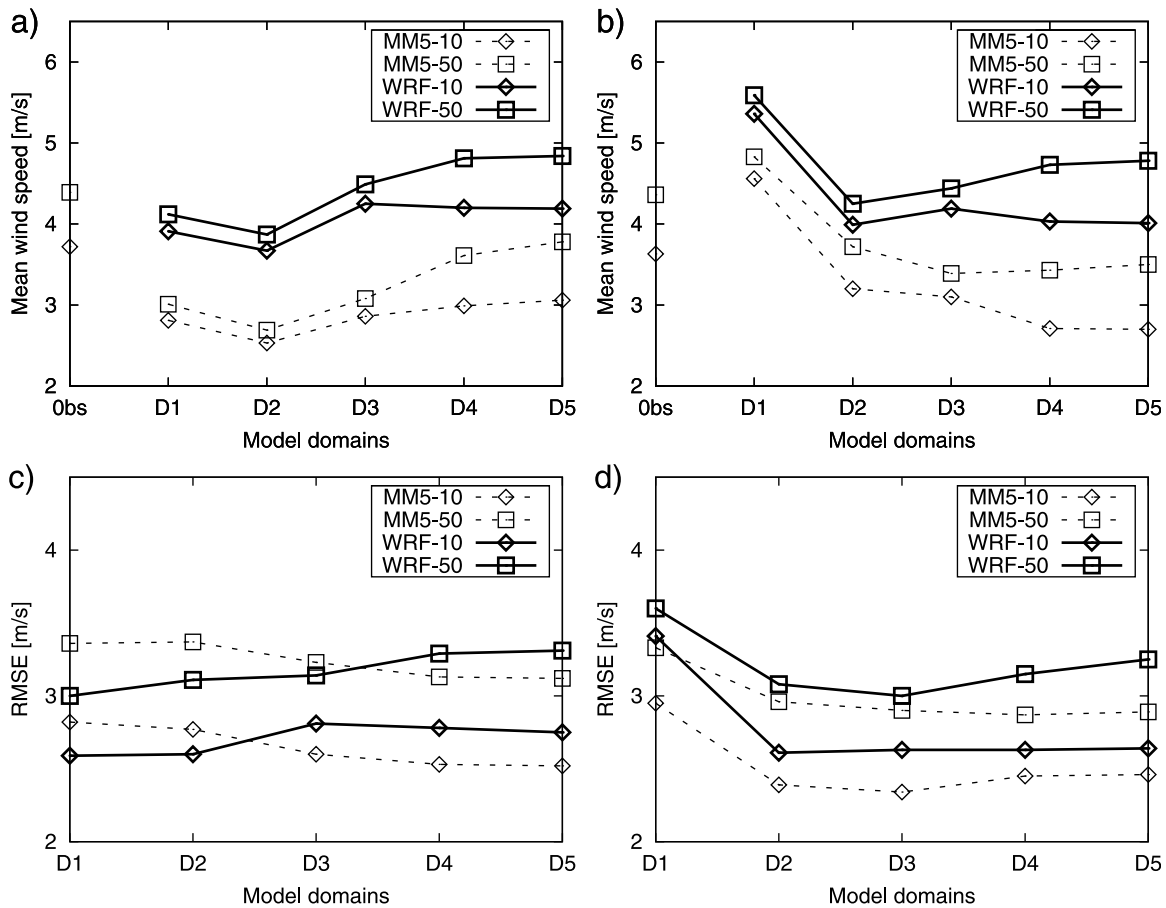
Figure 6. Mean wind speed in (a) July and (b) December 2007 and RMSE in (c) July and (d) December for all model domains for both MM5 and WRF models. On the *x* axis in Figures 6a and 6b "Obs" denotes observed values.

4.1. Moment-Based Verification

4.1.1. Bias and RMSE

[30] The systematic error referred to as the bias or the multiplicative bias (MBIAS), the percentage ratio of modeled to observed mean wind speed, and the root-mean-square error (RMSE) showed considerable differences between the two models (Figure 6). The major difference was that WRF showed larger magnitudes of mean wind speeds than MM5 (Figures 6a and 6b) in all domains. MM5 underestimated mean wind speeds at sub-kilometer grids by about −18% at 10 m AGL and −14% at 50 m AGL in July

and by about −26% at 10 m AGL and −20% at 50 m AGL in December (Figure 6 and Table 2). In contrast, WRF overestimated mean wind speeds by about 13% at 10 m AGL and 10% at 50 m AGL in July and by about 11% at 10 m AGL and 10% at 50 m AGL in December. The underestimation of MM5 and its larger bias magnitude in winter was noted in some recent high-resolution dynamical downscaling studies also over the sea surface where the model underestimated the near-surface winds for nearly −15% in July and −20% in January [*Hahmann et al.*, 2010]. On the other hand, WRF results for wind speed at 10 m AGL

Table 2. Horizontally Averaged Multiplicative Systematic Error (MBIAS) for MM5 and WRF in July and December 2007 for All Domains at 10 m and 50 m AGL[a]

	10 m AGL					50 m AGL				
	Domain 1	Domain 2	Domain 3	Domain 4	Domain 5	Domain 1	Domain 2	Domain 3	Domain 4	Domain 5
MM5 Jul	−24.6	−32.1	−23.1	−19.6	−17.8	−31.6	−38.8	−29.9	−17.8	−14.0
WRF Jul	4.9	−1.5	14.2	12.8	12.6	−6.3	−12.0	2.2	9.5	10.1
MM5 Dec	25.6	−11.8	−14.6	−25.5	−25.7	10.9	−14.7	−22.3	−21.4	−19.8
WRF Dec	47.6	9.8	15.5	11.2	10.5	28.3	−2.6	1.9	8.6	9.5

[a]Multiplicative systematic error (MBIAS) is calculated as a ratio of modeled and observed mean wind speed (in percent) for all domains (dmn1 is the outermost, dmn5 is the innermost). Results are horizontally averaged over all analyzed stations.

Table 3. Mean Monthly Observed and Simulated Wind Shear (s^{-1}) Between 50 m and 10 m AGL for MM5 and WRF in July and December 2007

				Domain			
	OBS	DMNS	1	2	3	4	5
Jul 2007	0.01678	MM5	0.00496	0.00401	0.00544	0.01552	0.01795
		WRF	0.00532	0.00496	0.00594	0.01529	0.01608
Dec 2007	0.01826	MM5	0.00694	0.01292	0.00717	0.01809	0.01999
		WRF	0.00592	0.00650	0.00627	0.01750	0.01910

differ from recent results achieved in the complex terrain of Spain, where the WRF model at 2 km grid spacing with somewhat different choice of parameterizations generally underestimated the daily mean wind speeds [*Jiménez et al.*, 2010]. Though the verification of daily means and hourly data may not be directly comparable, this suggests that mesoscale models may perform considerably different in different wind climates and with different model setups.

[31] As seen from the above values, MBIAS from both models for the verified months was higher at 10 m than at 50 m AGL. This implies that the source of the systematic model errors especially near the surface was likely due to the fidelity of the simulated land-atmosphere processes; that is, larger errors near the ground could be due to the quality and accuracy of the static lower boundary conditions (terrain and land-use), initialization of the soil variables, performance of the soil model, and the selection of parameters governing the vertical diffusion near the ground. Furthermore, though the decrease of the representativeness errors with height may be considered to partly account for better results at 50 m AGL, the consistency of results across domains and the small magnitude of representativeness errors in higher resolution domains suggest this issue may be of secondary importance.

[32] Further, the model performance was studied for the presence of a systematic/monotonous increase of accuracy with increasing the horizontal grid resolution. The most notable improvement was found for MM5 in July, when the systematic errors decreased with increased resolution. Nearly constant or slightly growing bias was found for WRF in July and for both models in December. Therefore, the systematic errors did not generally show monotonous decrease with the increased resolution in either model.

[33] Results from dmn1 (27 km grid) often considerably deviated from mean wind speed values and general bias trends of the other domains. This was very likely due to the fact that the static lower boundary conditions in dmn1 were not well resolved. The representation of terrain height in both models at all station locations in dmn1 was on average overestimated by 316 m (see section 3), while the crest height of the Sierra Nevada was almost halved. Due to the former, one may anticipate that this difference could result in simulating generally higher near-surface wind speeds. Weaker blocking of the westerly flow impinging on the windward side of the Sierra Nevada could be expected due to the underestimated crest height, which may considerably alter the simulated flow response and wind climate on the leeside. In consideration of the above, the accuracy of dmn1 is lower in December because a larger percentage of the energy is contained in LTD motions and a smaller percentage is related to diurnal flows. Therefore, the results from dmn1 should be interpreted with caution, even if they tend to apparently show higher accuracy than the results from the finer domains.

[34] The low-level wind shear is another important feature for simulating the near-surface winds with the desired accuracy. The mean monthly wind shear was calculated using mean monthly wind speeds at 10 m and 50 m AGL and equaled 0.017 s^{-1} (1.678 ms^{-1} over 100 m depth) in July and 0.018 s^{-1} (1.826 ms^{-1} over 100 m depth) in December. It can be inferred from Table 3 and Figures 6a and 6b that the magnitude of the MM5 and WRF simulated mean wind shear was generally three times smaller in dmn1, dmn2 (9 km grid) and dmn3 (3 km grid) than the observed estimate for both months. In contrast, the magnitude of the mean wind shear in both models was simulated quite accurately in dmn4 (1 km grid) and sub-kilometer domains (333 m grid). Therefore, both models were able to reproduce the mean monthly wind shear with the desired accuracy on a grid increment of 1 km or less. The accurate simulation of the mean wind shear is a notable benefit of dynamical downscaling at near-kilometer grid spacing. It should be mentioned that it is uncertain, however, how accurately the models reproduce the instantaneous wind shear, surface fluxes and their diurnal variability, which is beyond the scope of this analysis.

[35] The second most often used moment-based verification score is the RMSE, shown in Figures 6c and 6d. Though RMSE is more commonly used for verification of model forecasts, we found it to be useful for assessing the downscaled results and the benefits of increased resolution. The magnitude of the RMSE in July was similar for both models (Figure 6c) at both levels, while it was somewhat larger for WRF than for MM5 in December (Figure 6d). The RMSE values are comparable with the results achieved with other mesoscale models in complex terrain, such as the ALADIN [*Žagar et al.*, 2006]. The RMSE was generally greater at 50 m AGL, however, the RMSE normalized with the observed mean wind speed was similar at both levels. The RMSE in July generally showed a decreasing trend with increasing resolution for MM5 and increasing trend with increasing resolution for WRF. The RMSEs were nearly about the same for all domains in December, except for dmn1 which showed much larger values.

[36] To summarize, neither bias nor RMSE generally decreased with increasing grid resolution, which was noted in a number of high-resolution mesoscale modeling verification studies as discussed above. For example, *Rife and Davis* [2005] state that the improvement of higher-resolution domains is more evident with verification scores that account for realistic features in the modeled time series. In the subsequent sections, we shed light as to why the continuous moment-based scores such as bias or RMSE generally failed to show the systematic improvement with increased resolution as well as whether the benefit of higher-resolution modeling can be found using alternative verification measures.

4.1.2. Diurnal Variability

[37] The analysis of wind regimes in west-central Nevada (section 2) suggested that the moment-based scores could be noticeably influenced by the strong diurnal wind speed variability and the stability of the PBL. To investigate this in detail, the data is organized into separate bins for daytime
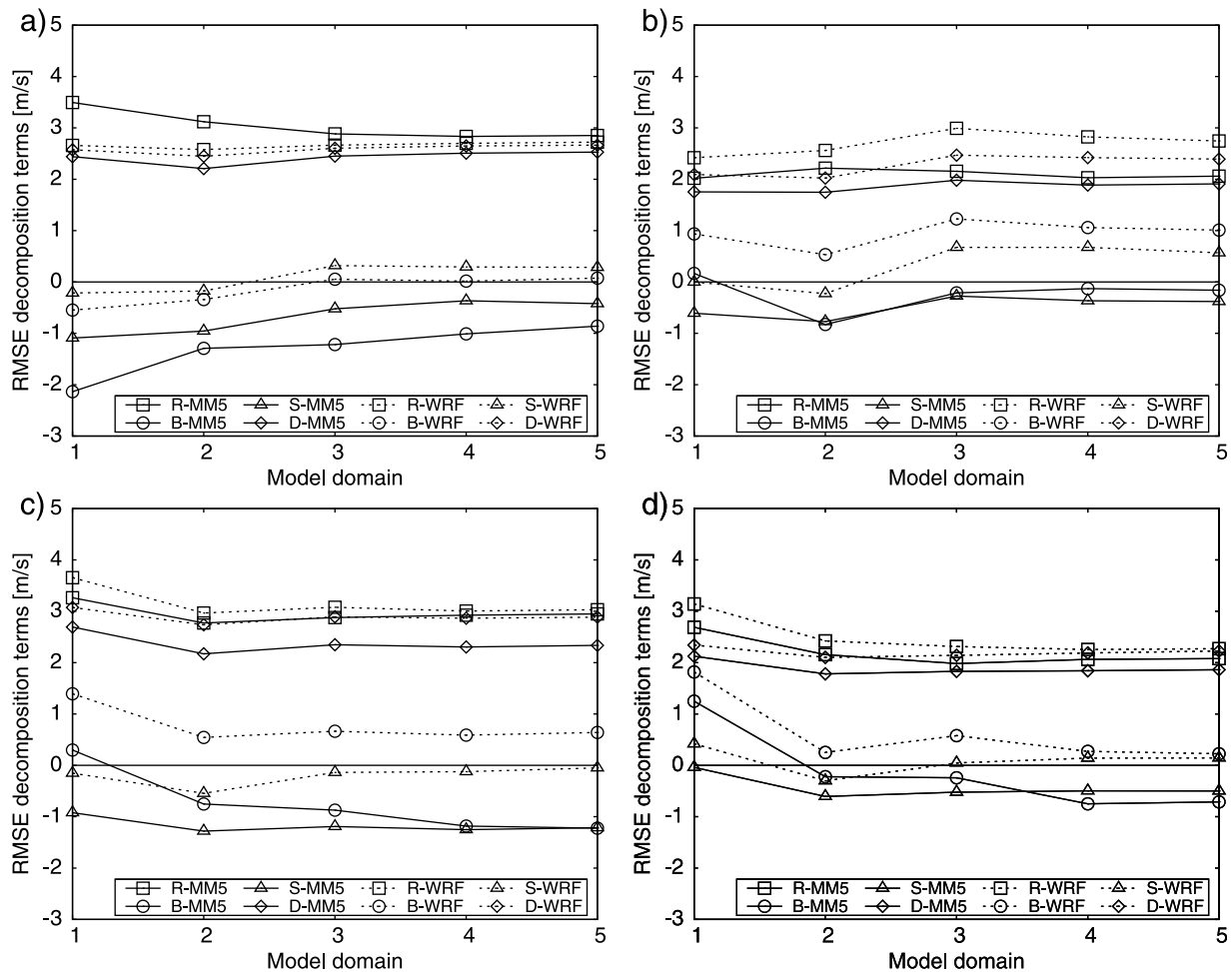
Figure 7. Decomposition of RMSE at 10 m AGL in July 2007 during (a) daytime and (b) nighttime and in December 2007 during (c) daytime and (d) nighttime for MM5 and WRF models. R- denotes the RMSE, B- denotes the bias of the mean, S- denotes the bias of the standard deviation and D- denotes the dispersion error.

(during 19–02 UTC ∼ 11–18 LST) and nighttime (during 06–13 UTC ∼ 22–05 LST), neglecting in-between transitional periods. The transitional periods are avoided to exclusively consider the well-mixed convective PBLs during the daytime and stably stratified PBL during the nighttime. This binning procedure provided also a larger data set for the analysis.

[38] Since the magnitude of the RMSE is affected by uncertainty both in space and time, the RMSE is decomposed into the following components: (i) bias of the mean (BM), (ii) bias of the standard deviation (BSD), and (iii) dispersion or phase error (DE) (see Appendix B for details). The components of the RMSE at 10 m and 50 m AGL are shown in Figures 7 and 8, and the corresponding MBIAS values are shown in Table 4. Results averaged over all stations showed that regardless of the month or part of the day, the RMSE generally did not decrease with increased resolution; the few exceptions are MM5 during daytime in summer and WRF during nighttime in winter. The largest part of the RMSE was due to phase error regardless of the month, level or period of the day. On the other hand, the

biases of the mean and standard deviation were several times smaller in magnitude than the phase error.

[39] Furthermore, the relative contribution of the DEs to the RMSE generally increased, while the relative contribution of the BMs and BSDs to the RMSE generally decreased with the increased resolution. Such large phase errors are commonly found in numerical weather forecasts where uncertainties in lateral boundary conditions (LBCs) are the primary source of the forecast errors [*Anthes et al.*, 1989; *Warner et al.*, 1997]. The magnitude and presence of DE regardless of the wind regimes in the two analyzed months suggests that the LBCs are still the major source of phase errors. However, the length of simulations (36 h) is generally not long enough to allow for LBCs to propagate from the outer boundaries of the outermost domain to wind tower locations. Nevertheless, the time-evolution of the near-surface model solutions might have also allowed for DE growth from the following: (i) inaccurate simulations of westerly flow blocking, frontal retardations, and scales and magnitudes of the thermally driven flows, due to inadequate representation of the major mountain ranges that are not well
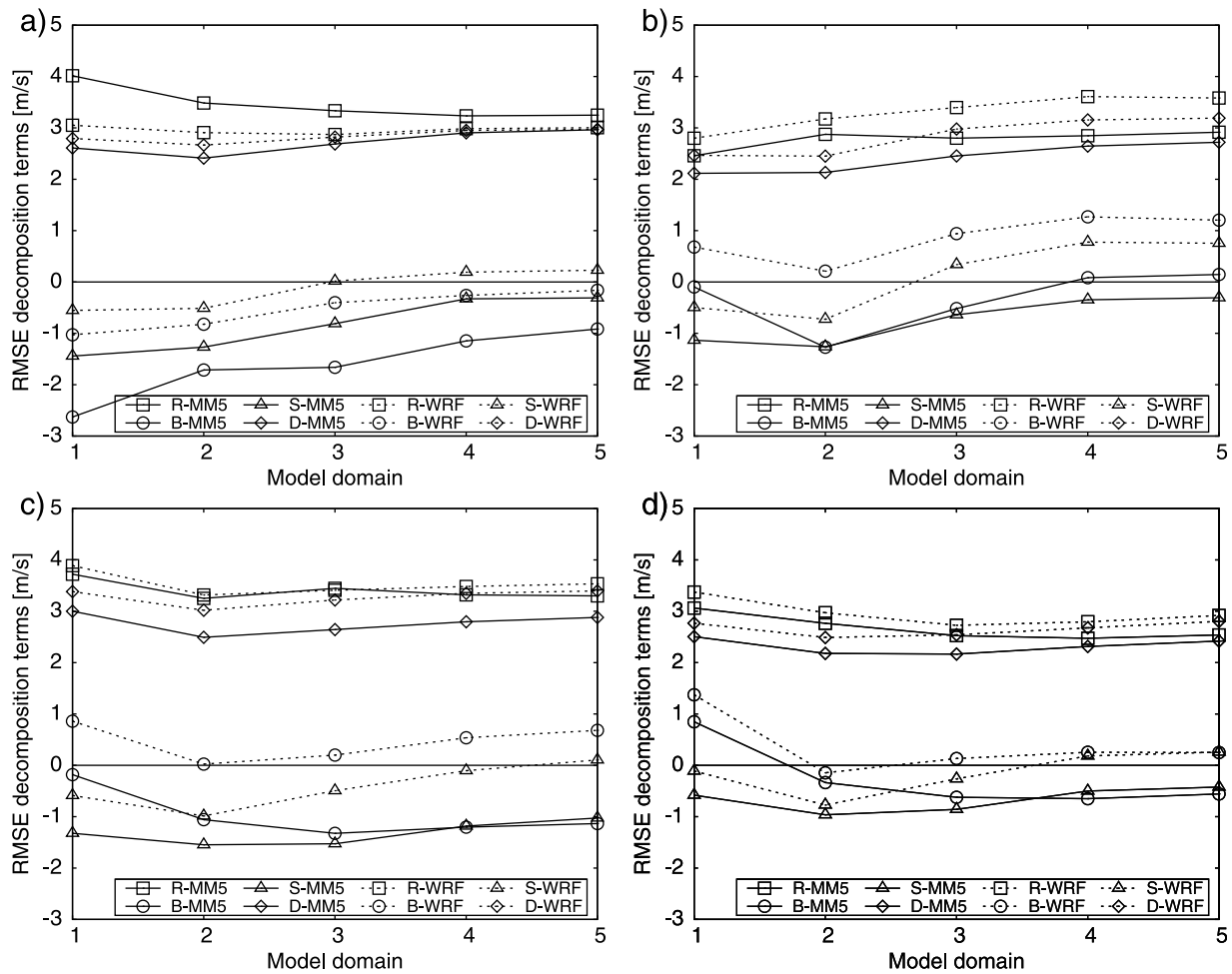
Figure 8. Decomposition of RMSE at 50 m AGL in July 2007 during (a) daytime and (b) nighttime and in December 2007 during (c) daytime and (d) nighttime for MM5 and WRF models. R- denotes the RMSE, B- denotes the bias of the mean, S- denotes the bias of the standard deviation and D- denotes the dispersion error.

resolved in our model setup. E.g., the flow over the Sierra Nevada is in our model setup simulated only in dmn1 and dmn2, in which the main terrain features are still inadequately resolved. Therefore, this is the issue of the nested

LBCs, that is the WRF simulated LBCs for the nested domains, (ii) the accuracy of the land-surface model, especially the soil moisture, which might induce large DE since it determines the times of the onset and decay of the diurnal

Table 4. Daytime and Nighttime Horizontally Averaged Multiplicative Systematic Error (MBIAS) for MM5 and WRF in July and December 2007 for All Domains at 10 m and 50 m AGL[a]

	10 m AGL					50 m AGL				
	Domain 1	Domain 2	Domain 3	Domain 4	Domain 5	Domain 1	Domain 2	Domain 3	Domain 4	Domain 5
MM5 Jul day	−46.3	−28.0	−26.4	−21.9	−18.6	−51.0	−33.3	−32.3	−22.3	−17.8
WRF Jul day	−11.9	−7.4	1.2	0.4	1.6	−20.0	−16.0	−7.8	−5.1	−3.1
MM5 Jul night	5.7	−28.2	−7.3	−4.4	−5.4	−2.7	−35.3	−14.4	2.3	4.1
WRF Jul night	31.9	18.1	41.8	36.1	34.4	18.9	5.9	26.2	35.3	33.5
MM5 Dec day	6.8	−17.3	−20.0	−27.1	−28.1	−3.6	−20.8	−26.0	−23.6	−22.3
WRF Dec day	32.0	12.5	15.2	13.5	14.7	16.9	0.5	3.9	10.5	13.4
MM5 Dec night	39.1	−6.9	−7.6	−23.5	−22.3	22.0	−8.7	−16.1	−16.8	−14.4
WRF Dec night	56.9	7.9	18.1	8.5	7.0	35.6	−3.8	3.4	6.6	6.5

[a]Multiplicative systematic error (MBIAS) is calculated as a ratio of modeled and observed mean wind speed (in percent) for all domains (dmn1 is the outermost, dmn5 is the innermost). Data is separated into daytime (11–18 local time) and nighttime (22–05 local time) bins. Results are horizontally averaged over all analyzed stations.

flows and evolution of the planetary boundary layer, and iii) the appropriateness of the physical parametrizations, such as related to evolution of the PBL and potential phase errors related to the transitions between its nocturnal and convective phases. In all of these scenarios, the increased realism of the higher-resolution simulations would further contribute to increasing the DE. Therefore, the contention of realism from the higher-resolution simulations is better justified if the dispersion error growth is rather clearly understood. The use of spectral nudging of larger-scales toward the reanalysis data [*von Storch et al.*, 2000], more frequent update of LBCs, the land-soil model initialization, and carefully chosen domain configurations incorporated with finer topographic and land/soil use details have potential to reduce the phase errors in the dynamical downscaling of the near-surface winds in complex terrain.

[40] During the daytime in July (Figures 7a and 8a), MM5 showed somewhat larger RMSEs than WRF at both 10 m and 50 m AGL. This difference was apparently larger for the coarser domains (dmn1, dmn2) due to the larger negative biases of the mean and standard deviation for MM5 than for WRF. In the higher resolution domains (dmn3, dmn4, and dmn5), MM5 biases decreased and the RMSEs of WRF were almost exclusively composed of phase errors; the correlations improved to 0.5 for WRF and 0.4 for MM5 (not shown). These correlation values are somewhat lower than over the ocean surface. For example, the evaluation of the MM5 model at 9 km grid spacing with buoy stations near the U.S. West Coast showed that correlations in June were generally between 0.5 and 0.7 [*Koracin and Dorman*, 2001]. The daytime biases of mean and standard deviation in both models at both levels generally decreased with increased resolution. This clearly suggests that the presence of strong diurnal daytime forcing acts to systematically enhance the accuracy of mesoscale model results at finer horizontal grid resolutions.

[41] During the nighttime in July, all three RMSE components were larger for WRF than for MM5 (Figures 7b and 8b) at the finest resolution (dmn5). For WRF, contributions to RMSEs besides the DEs were considerably larger during nighttime than during the daytime. Table 4 shows that the multiplicative bias of the mean in the WRF results increased with the grid spacing and reached almost 35% in dmn5 at both analyzed levels, which was the largest WRF bias found regardless of the month or period of the day. On the other hand, MM5 biases generally decreased with increased resolution. This was more evident at 50 m AGL, where, for example, the multiplicative biases of the mean reached were 2.3% and 4.1% for domains dmn4 and dmn5 respectively. Therefore, the accuracy of the simulated nocturnal circulations associated with the thermally driven flows in MM5 improved with the increased resolution. On the other hand, the WRF simulations of nocturnal flows were less accurate, overestimating their strength and temporal variability over the area. The somewhat lower correlations of both models were found in July during the nighttime than during the daytime.

[42] In December, the RMSEs were generally similar for both models. All three RMSE components were of smaller magnitude during the nighttime than during the daytime (Figures 7c, 7d, 8c, and 8d). The DEs were smaller and the BMs and BSDs were larger for MM5 than for WRF during

both daytime and nighttime. Neither model showed improvement in the BM or MBIAS with increased resolution (Table 4). However, the BSD generally decreased with increased resolution for both models, especially at 50 m AGL. Finally, correlations were higher in December than in July for both models, reaching 0.65 during daytime and 0.55 during nighttime. Over both months, the correlation values were similar to those found in other high-resolution dynamical downscaling studies. For example, the MM5 modeled winds in the cold season over the southern California at the 6 km grid spacing reached correlations 0.5–0.75 [*Conil and Hall*, 2006].

[43] To summarize, the changes in moment-based scores with increasing resolution were highly dependent on the nature of the diurnal flows. The dispersion error was the primary contributor to the RMSE, and its relative contribution to the RMSE generally increased with increased resolution. If the diurnal flows contained a considerable part of the observed energy such as in July 2007, WRF showed lower BM and BSD than MM5 during the daytime and higher BM and BSD during nighttime. In December 2007, when the observed energy associated with the diurnal and sub-diurnal flows was negligible, WRF showed smaller BM and BSM than MM5 regardless of the period of the day. The most notable improvement with increased resolution was found for the BSD, i.e., for the temporal variability of the wind during the analyzed months as well as daytime and nighttime. This improvement was found to be more monotonous at 50 m AGL than at 10 m AGL where flow dynamics are less affected by microscale effects associated with the local topography. On the other hand, the improvement of the bias of the mean with increased resolution was found only during daytime in July in the presence of daytime diurnal flows. Thus, the moment-based verification suggests that improvement in the simulated temporal variance of the wind speed and mean wind shear seem to be the most universal benefits of the increased horizontal resolution in the process of dynamical downscaling.

4.1.3. Wind Speed Distributions

[44] The comparison of measured and simulated wind speed distributions, as a part of the moment-based verification, provide an additional insight into the model performance that is insensitive to phase errors. Due to the importance of diurnal flows over the target area in summer and the differences in model accuracy between summer and winter, we performed the analysis separately for daytime and nighttime periods (as in section 4.1.2) focusing on the most pronounced deficiencies of the MM5 and WRF models as seen in previous sections.

[45] The simulated wind speed histograms averaged over all stations at 10 m and 50 m AGL were calculated using 2 ms^{-1} bins. The results were qualitatively similar at these levels and the errors were quantitatively somewhat smaller at 50 m AGL; therefore, for brevity, we are only showing results at 10 m AGL. During July, MM5 results were less accurate than WRF results during the daytime and more accurate during the nighttime (Figure 9). The most notable MM5 feature is a considerable underestimation of the frequency of stronger daytime winds ($V > 6$ ms^{-1}) in the finest grids (Figure 9a). Thus, the negative MM5 bias during the daytime was apparently due to underestimation of the frequency of stronger winds. Also, the model largely
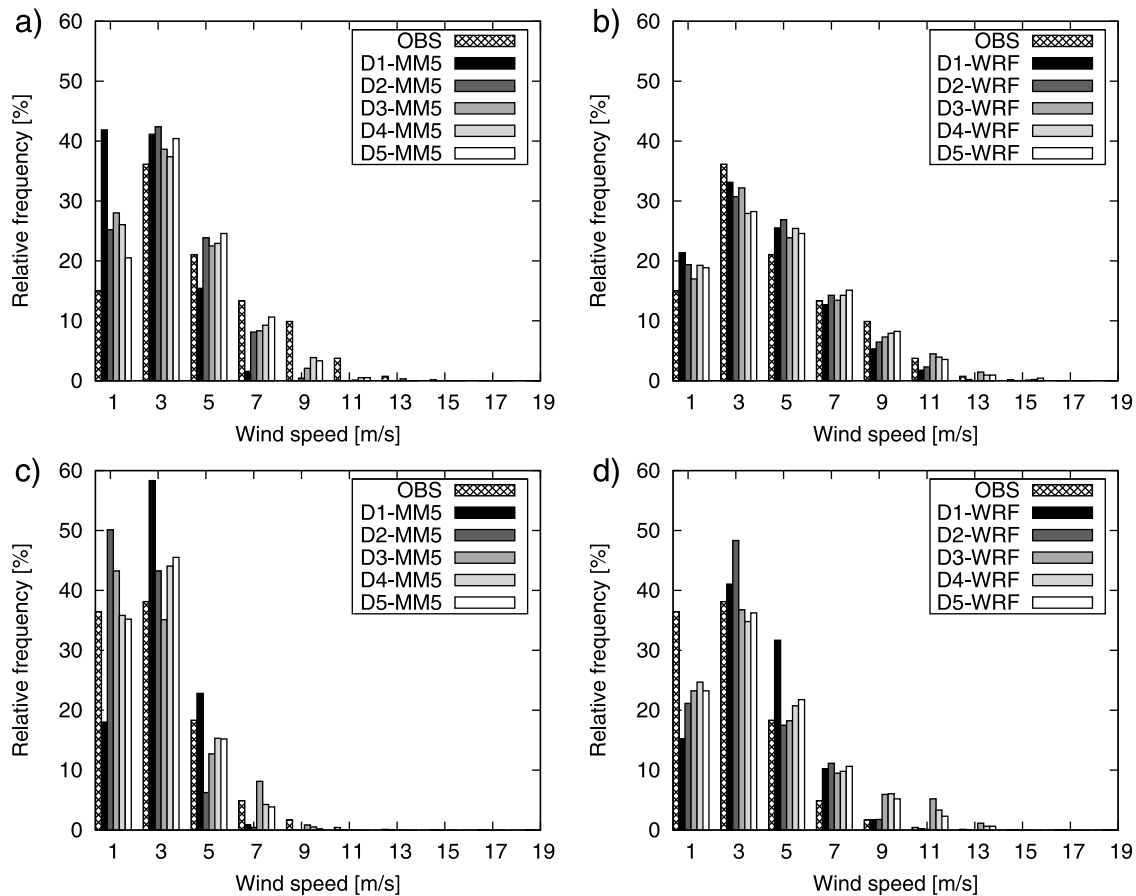
Figure 9. Histograms of observed and modeled wind speed at 10 m AGL during daytime with (a) MM5 and (b) WRF and during nighttime with (c) MM5 and (d) WRF in July 2007. D1 denotes domains 1, D2 domain 2, D3 domain 3, D4 domain 4 and D5 domains 5.

overestimated the frequency of the weakest winds (<2 ms^{-1}). The better performance of MM5 during nighttime in accordance with the high-resolution modeling study over the eastern Mediterranean coast, where verification of the MM5 simulations at 5 km grid spacing using two wind towers suggested that the model results were more accurate during nighttime than during daytime [*Hahmann et al.*, 2010]. Nevertheless, the improvement with increasing resolution in MM5 was clearly found for stronger winds during the daytime, while there was no systematic enhancement of accuracy with increased resolution during the nighttime.

[46] The wind speed distribution from WRF (Figures 9b and 9d) was generally in better agreement with the measured distribution during the daytime; however, it largely overestimated the frequency of the stronger winds and underestimated the frequency of the weaker winds at finer resolutions during the nighttime. Thus, the positive WRF bias during the nighttime (see section 3.1) was apparently tied to overestimation of the frequency of stronger winds. Similar to our finding, considerable inaccuracies associated with WRF simulations of nocturnal low-level jets were found with respect to the height, intensity, and vertical structure [*Storm et al.*, 2009]. Finally, the WRF underestimation of the frequency of the weakest winds could be likely due to excessive diffusion under near-calm conditions that is

typically an artifact found in mesoscale models for numerical stability and to reduce unrealistic cold pool formation near the surface [*Cuxart et al.*, 2006].

[47] During December, MM5 somewhat underestimated the stronger winds and this underestimation was higher during the day (Figure 10). Since the strength of the diurnal motions in winter was quite weak, the underestimation, found in both analyzed months and at both levels, was apparently not due to erroneous simulations of thermally driven flows. Rather, it may be related to the overall model spectral kinetic energy. This is discussed in the next section. It is notable that WRF distributions of strong nocturnal winds in December were in good agreement with the observed values. This suggests that the WRF errors were primarily associated with the accuracy of simulating the thermally driven stably stratified nocturnal flows.

4.2. Spectral Verification

[48] Besides standard statistical verification, complementary model verification was also performed using spectral analysis, since it is scale-selective and enables a physical insight into the model performance. In addition to the analysis of spectral density functions, which is often used for the qualitative assessment of model performance, the spectral analysis may provide a quantitative measure of the model
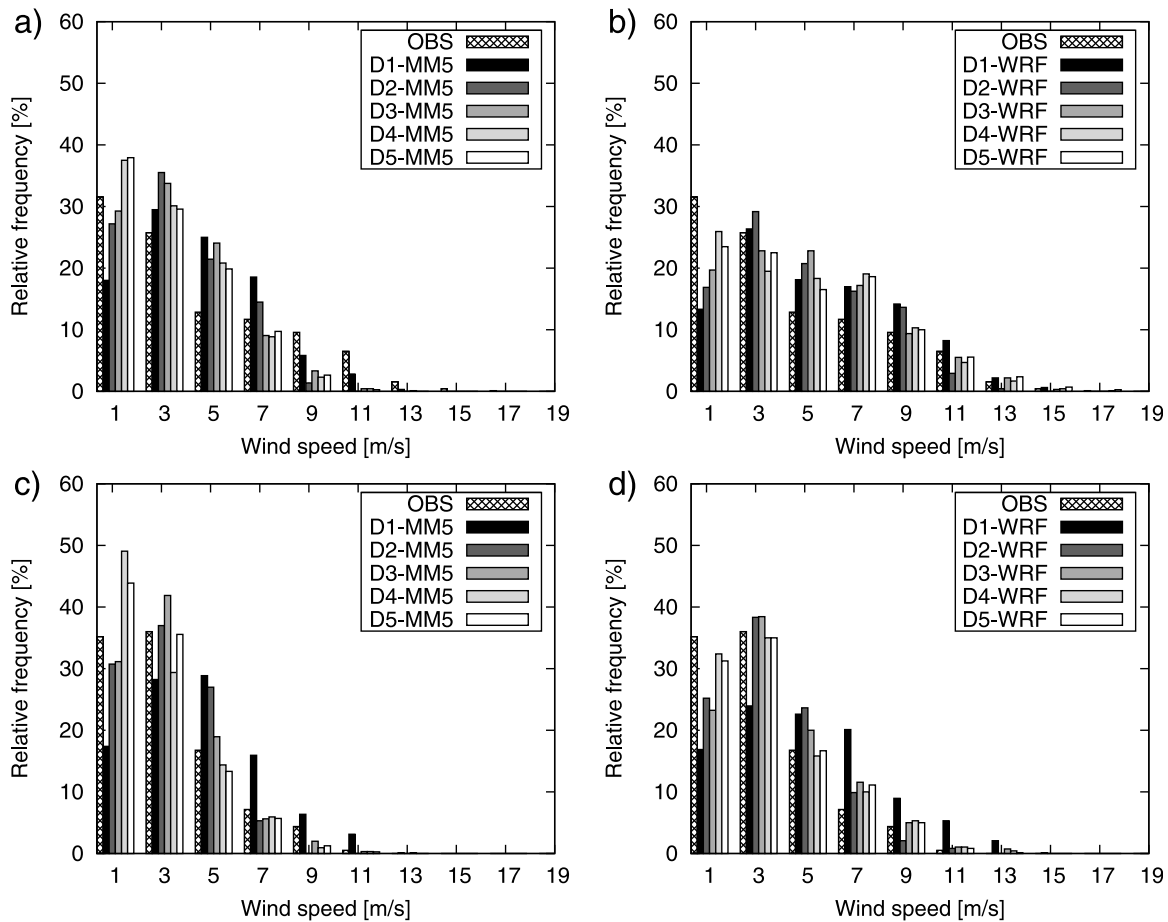
Figure 10. Histograms of observed and modeled wind speed at 10 m AGL during daytime with (a) MM5 and (b) WRF and during nighttime with (c) MM5 and (d) WRF in December 2007. D1 denotes domains 1, D2 domain 2, D3 domain 3, D4 domain 4 and D5 domains 5.

accuracy. As described in section 2 and Appendix A, the motion spectrum is divided into three classes: sub-diurnal (SD, 2 h < T < 22 h), diurnal (DI, 22 h < T < 26 h) and longer-than-diurnal (LTD, 26 h < T < 7 d). The benefit of such analysis is to derive a physically meaningful and phase error-tolerant spectral verification measure. Comparison of the MM5 and WRF model results in spectral space was performed using hourly data as used in the statistical verification.

[49] In July 2007, the percentage ratio of the modeled and observed spectral kinetic energies in the total, LTD, DI and SD frequency ranges considerably varied at 10 m and 50 m AGL in all the domains for both models (Figure 11). In the total and LTD range, the spectral kinetic energy from dmn1 was larger than for dmn2, and this is likely due to inconsistencies in the representation of the modeled and true orography as discussed in sections 3 and 4.1.1. The results from the higher resolution WRF domains (dmn4 and dmn5) generally yielded better results than MM5 in the total, LTD, and DI ranges. While for WRF the energy contained in these frequency bands was close to observations, the higher resolution domains of MM5 contained approximately 50% of the observed spectral kinetic energy at 10 m AGL in the total and LTD frequency bands and about 35% in the DI frequency band. Somewhat improved results were found at

50 m AGL. Finally, the energy of SD motions in the higher resolution domains was overestimated by about 70% at 10 m AGL and 40% at 50 m AGL in WRF, whereas it was underestimated by about 30% of the observed value at both levels in MM5. It is very likely that the WRF overestimation of the strength of SD motions resulted from the large positive WRF BSD during nighttime in July (see also section 4.1.2). Thus, the overestimation of nocturnal temporal wind speed variability can be associated with the overestimation of the spectral kinetic energy of the SD motions.

[50] Generally, increasing the horizontal grid resolution in July showed a considerable benefit, which was more evident in simulating winds at 50 m than 10 m AGL. The accuracy of the WRF results in the DI band showed the largest increase with increasing resolution at both levels. The MM5 results in the DI band improved as well, especially at 50 m AGL, but the errors remained large. The DI band results of MM5 suggest that the MM5 setup, such as the choice of physical parameterizations, was not conducive to simulating the diurnal variability of thermally driven winds in the study region. Further, it is unclear to what extent the use of a 5-layer slab model in MM5 contributes to the lack of energy of diurnal flows as compared to the Noah land surface model used in WRF. Finally, the accuracy of the WRF model in
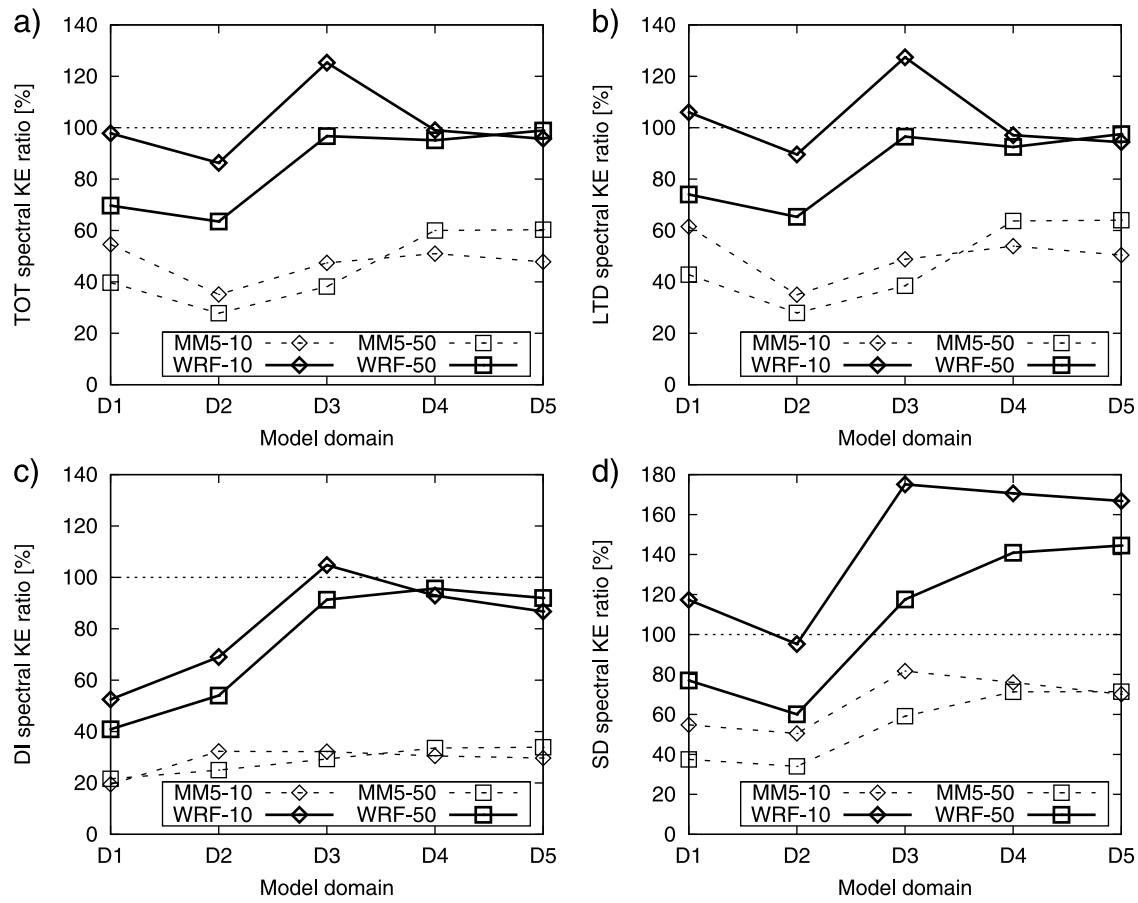
Figure 11. Variability of the ratio (in percent) of modeled and observed integrated spectral kinetic energy (horizontally averaged over all measurements stations) for all computational domains for MM5 and WRF models in (a) total range of frequencies (TOT, 2 h < t < 7 d), (b) longer-than-diurnal range (LTD, 26 h < t < 7 d), (c) diurnal range (DI, 22 h < t < 26 h) and (d) sub-diurnal range (SD, 2 h < t < 22 h) at 10 m and 50 m AGL for July 2007. A perfect match (100%) is plotted as a short-dashed line.

kilometer- and sub-kilometer-resolution domains in the LTD and DI ranges clearly suggests that improvement of results with increasing the horizontal resolution is found for domains down to kilometer grid spacing. Therefore, at least a kilometer grid spacing in the horizontal is required to obtain reliable simulations of the energy associated with LTD and DI motions. The added value of sub-kilometer grid spacing, however, was not that obvious in our study at one hand likely due to inappropriateness of physical parametrizations, as discussed earlier. Furthermore, it is not obvious to what extent this is due the restrictive size of sub-kilometer domain geometries since in this case the lateral boundary conditions of the parent domain largely determine the model solutions. In addition, several studies in complex terrain showed that the near-surface wind in the very-high resolution domains mostly adopts to the orography [*Žagar et al.*, 2006; *Horvath et al.*, 2011] irrespective of the domain size. Therefore, the introduction of motions in sub-kilometer domains which were unresolved in the domain with a kilometer grid spacing may occur as expected, but those motions may contain low or negligible portion of the total energy variance.

[51] During wintertime in December 2007, most of the spectral kinetic energy was contained in the LTD frequency band, so the strengths of the total and LTD motions were almost equal (Figure 12). Results from the higher resolution domains (dmn4 and dmn5) were more accurate for WRF than for MM5, since MM5 considerably underestimated the energy in these bands. In the low-energy DI and SD frequency bands, the model accuracies were comparable and the models showed similar biases but of opposite signs. Similar to those found for statistical verification, processes in dmn1 were generally more energetic than in dmn2, both in total and in the LTD bands. By not considering dmn1 in the analysis, the WRF results at 50 m AGL systematically improved with increasing resolution, except for the finest grid. The WRF results at 10 m AGL from all domains (excluding dmn1) were accurate, and consequently showed little improvement with increasing resolution. Thus, the best WRF results in the primary energy-containing total and LTD bands in December were found for dmn4 at both levels. On the other hand, the improvement with increased resolution in these bands for MM5 was less obvious and the analysis of the benefit of increasing horizontal resolution generally yielded mixed results.
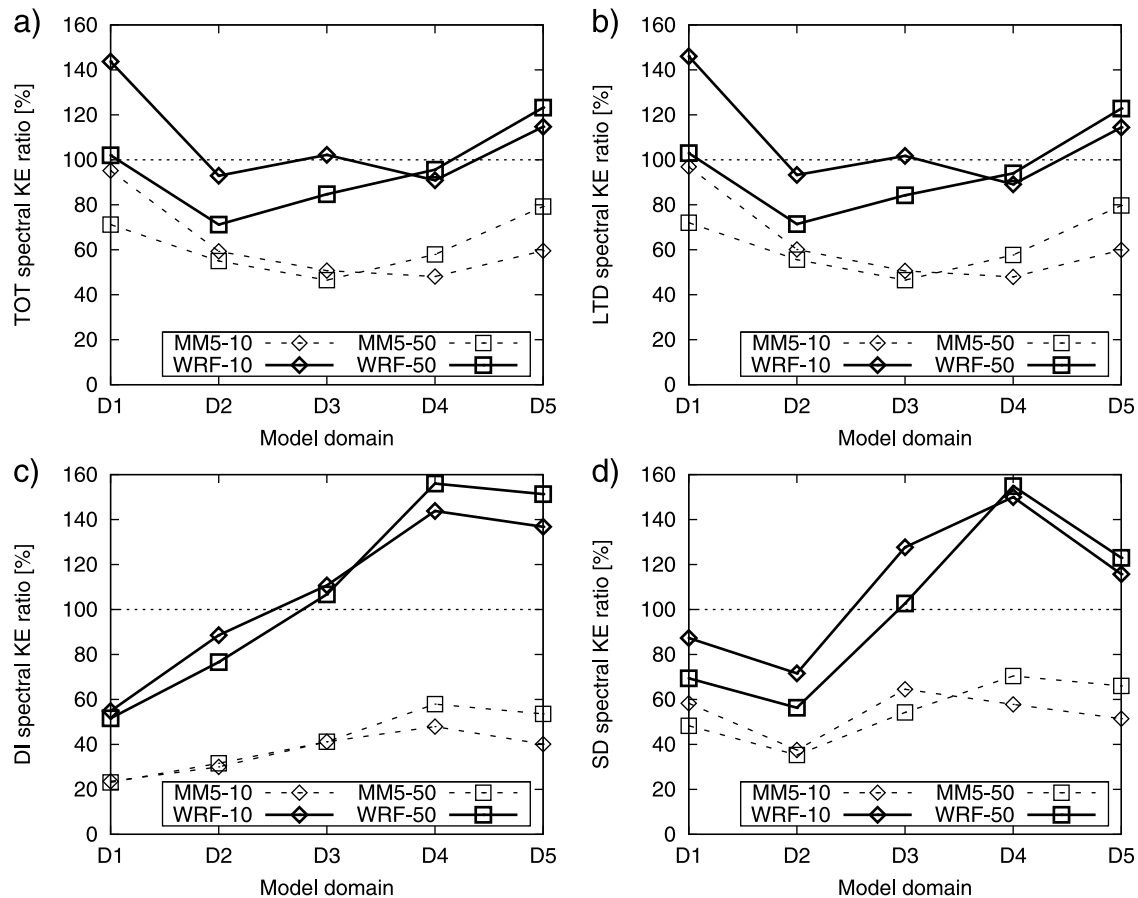
Figure 12. Variability of the ratio (in percent) of modeled and observed integrated spectral kinetic energy (horizontally averaged over all measurements stations) for all computational domains for MM5 and WRF models in (a) total range of frequencies (TOT, 2 h < t < 7 d), (b) longer-than-diurnal range (LTD, 26 h < t < 7 d), (c) diurnal range (DI, 22 h < t < 26 h) and (d) sub-diurnal range (SD, 2 h < t < 22 h) at 10 m and 50 m AGL for December 2007. A perfect match (100%) is plotted as a short-dashed line.

[52] The spectral performance evaluation suggested that the WRF results were more accurate than MM5 in an overall sense. For both models, the gain with increasing resolution was more systematic in July than in December and at 50 m AGL than at 10 m AGL. This suggests that the improvement in the accuracy of the static lower boundary condition does not necessarily improve the model performance per se, but that it requires a more adequate specification of the state of the land-surface – atmosphere intermediary. For example, improved data assimilation of soil variables and a more realistic specification of near-surface vertical mixing during stratified nocturnal flows are some of the issues that need to be addressed further toward a systematic improvement of the dynamical downscaling process with the increased horizontal grid resolution.

5. Conclusions

[53] In this study, sub-kilometer dynamical downscaling with the Mesoscale Model 5 Version (MM5) and the Weather Research and Forecasting (WRF) model was performed with an aim to examine: i) the accuracy and main strengths and weaknesses of the mesoscale models to reproduce the near-surface winds over the complex terrain of west-central Nevada, and ii) the impact of horizontal resolution on the models' accuracy and the equivalence of moment-based and spectral verification metrics. The models were configured with seven domains whose horizontal resolutions ranged from 27 km to 333 m. The simulated winds at 10 m and 50 m AGL for July and December 2007 were verified in both physical (temporal) and spectral space against the measurements collected at four 50-m meteorological wind towers located in the complex terrain of west-central Nevada.

[54] The in situ measurements and NARR reanalysis showed that the wind regimes in these two months were predominantly bi-directional, but with distinctly different underlying causes. In July, the wind regime is characterized by strong thermally driven diurnal circulations that develop under the quasi-stationary upper-level ridge. The contribution of observed diurnal flows in July was spectrally evaluated by separating the motions into the following frequency bands: longer-than-diurnal (LTD), diurnal (DI) and sub-diurnal (SD) frequency ranges. These frequency bands accounted for ~80%/15%/4% of the total observed spectral kinetic energy respectively. In December, the strength of the

DI and SD flows was nearly negligible adding up to ~3% of the total spectral kinetic energy and almost all of the energy was contained in motions of synoptic and longer-than-diurnal mesoscale periods.

[55] Verification of systematic errors suggested that the performance of the MM5 and WRF models was considerably different. In both months, simulated mean wind speeds were higher for WRF than for MM5 for all domains and at both analyzed levels. At 10 m AGL, the model results showed the negative biases of −18% in July and −26% in December for MM5 and positive biases of 13% in July and 11% in December for WRF. This indicates that a dynamical down-scaling approach combining two or more models, that is the ensemble approach to dynamical downscaling, might have a potential to improve the results. At 50 m AGL, the absolute values of biases were smaller for close to 20% compared to the biases at 10 m AGL. This suggests that one of the primary sources of near-surface wind speed errors is related to the lower boundary condition and the representation of the land-atmosphere interaction in the surface layer. The RMSEs were of similar magnitudes for both models. Gen-erally, neither biases nor RMSE systematically improved with reducing the grid spacing. Mean wind shear between the 10 m and 50 m AGL, however, was in both months and for both models well simulated and substantially improved with resolution, thus highlighting the clear benefit of the performed dynamical downscaling at kilometer and sub-kilometer resolutions.

[56] Decomposition of the RMSE showed that dispersion or phase errors were the primary sources of errors regardless of the model, the analyzed month or the period of the day, and that their contribution grew with the resolution. The relative contribution of phase errors to the RMSE was larger for WRF than for MM5. The relative contributions of other components to the RMSE, that is the bias of the mean and bias of the standard deviation, generally diminished with decreasing grid spacing. It is likely that large phase errors are primarily introduced by i) the errors introduced through the lateral boundary conditions of the parent domains ii) lower boundary conditions and the physics options that control evolution of the onset of thermally driven flows and the planetary boundary layer, such as the soil moisture initi-alizations, the land-soil model and the planetary boundary layer parameterizations. Furthermore, the performance of the models is strongly influenced by the presence and type of diurnal circulations. In July, during a convective daytime PBL, kilometer- and sub-kilometer-resolution domains gen-erally performed better for WRF than for MM5 at both ana-lyzed levels. While WRF showed no considerable errors, the MM5 performance was characterized by large negative bias of the mean (−20%), negative bias of the standard deviation, and underestimated frequency of stronger daytime winds. However, MM5 performed more satisfactorily for stably stratified/nocturnal PBL conditions than WRF, which over-estimated the frequency of stronger nocturnal winds resulting in overall positive bias of 35% of the mean wind speed and a large overestimation of temporal wind speed variability. Indeed, the inaccuracy of simulations of nocturnal thermally driven flows in July were shown to be the main weakness of the WRF model. In December, when the energy of diurnal flows is small, the results were more coherent throughout the period of the day. For the highest resolution domains, the

biases of the mean were generally close to −25% for MM5, primarily due to underestimation of the frequency of stronger winds, and 10% for WRF. This clearly shows that the over-estimation of thermally driven nocturnal flows is one of the main deficiencies of the WRF model and suggests that underestimation of the overall spectral kinetic energy of motions is present in the MM5 model.

[57] The presence and type of diurnal flows considerably affects the improvement of the models' accuracy with increasing resolution. The most prominent improvement in July was found for the bias of the mean for both models during convective daytime PBL. During the nighttime, however, results improved with resolution for MM5, but not for WRF. In contrast, neither model showed improvement of bias of the mean during December regardless of the period of the day. Likewise, the accuracy of the simulated wind speed distributions was found to improve more clearly in July. This suggests that improvement of mesoscale model accuracy with horizontal resolution is more obvious if the resolved scales added by the higher resolution contain a considerable part of the energy, such as for thermally driven flows. For the bias of the standard deviation, however, an improvement with resolution was found for both models, both months and regardless of the period of the day (except for the WRF overestimation during July nighttime). Thus, improvement in simulating the temporal variance of wind speed seems to be one of the most universal benefits of higher resolution dynamical downscaling. Finally, the reduction of the bias of standard deviation, as well as bias of the mean when it existed, was again found to be more systematic at 50 m than 10 m AGL.

[58] Quantitative spectral verification metrics in July show that the WRF results from the kilometer- and sub-kilometer-resolution domains, unlike the domains with coarser grid spacing, were almost identical to observed values of spectral kinetic energy in the total, LTD, and DI frequency bands at both 10 m and 50 m AGL. The corresponding MM5 results, on the other hand, underestimated spectral kinetic energy and equaled close to 55% of the observed values in total and LTD frequency ranges and almost 40% in the DI range. In contrast, MM5 showed better accuracy in the SD band than WRF, which largely overestimated the atmospheric sub-diurnal variability. It is very likely that this excessive sub-diurnal variability is related to the WRF overestimation of the bias of standard deviation in July nighttime. In December, when the energy of periodic motions was almost entirely contained in the LTD band, WRF outperformed MM5 in the total and LTD frequency bands and showed comparable magnitudes in the DI and SD frequency bands. Therefore, WRF is showing overall better performance in energy-containing frequency bands than MM5, which generally tends to underestimate the observed energy variance spec-trum at all temporal scales.

[59] The improvement of the models' accuracy with res-olution was found in the spectral space as well. This improvement, though not systematic, was more evident at 50 m than at 10 m AGL and therefore, results of the moment-based and spectral verifications were alike. Gener-ally, the improvement was more pronounced for the fre-quency bands with a considerable portion of the energy, such as the LTD band in both analyzed months and the DI band in July. Among these bands, the most prominent

improvement for both models was found for DI band in July, especially for the WRF model. It should be pointed out that due to the increasing errors when approaching the ground, more detailed evaluation of the near-surface model accuracy would be achieved by providing soil and turbulence flux measurements, which might more clearly point out the main model deficiencies.

[60] In general, the WRF model was superior and showed more accurate results for dynamical downscaling than MM5 (though with some exceptions, such as simulations of nocturnal diurnal flows during summer). Both the moment-based and spectral verifications suggest that the results for kilometer- and sub-kilometer domains (grid spacing of 1 km and 333 m, respectively) were generally of higher accuracy than for the domains with 27 km, 9 km and 3 km grid spacing, especially if the diurnal flows were a significant feature of the wind regime. Furthermore, in our study the sub-kilometer grid spacing did not generally improve the results from the kilometer grid spacing. In other words, the improvement of results with increasing the resolution was generally found for domains down to a kilometer grid spacing, while domains with sub-kilometer grid spacing did not further improve the accuracy of the results. Therefore, this study suggests that a near-kilometer horizontal grid resolution of the current state-of-the-art mesoscale models is necessary, and perhaps optimal, for reliable dynamical downscaling of near-surface wind speed climate over complex terrain similar to that of west-central Nevada.

Appendix A

A1. Spectral Verification Metrics

[61] The approach for quantitative spectral verification can be summarized as follows: i) the spectral density functions (variance spectra) were calculated using observed and modeled time series of wind speed, and ii) contributions to the wind speed variance of a given frequency band, i.e., the spectral kinetic energy of periodic motions of the given frequency band, were calculated by integrating the spectral density functions over the given frequency range. As described earlier, we divide the motion spectrum into three classes: sub-diurnal (SD, 2 h < T < 22 h), diurnal (DI, 22 h < T < 26 h) and longer-than-diurnal (LTD, 26 h < T < 7 d), and the associated integration of the spectral density functions is performed as follows:

$$E_i = \int_{f(T_i)}^{f(T_{i+1})} S(f)\,df \;\; ; i = 1, 3 \tag{A1}$$

where E_i is the spectral kinetic energy of periodic motions in a chosen frequency band, S is the spectral density function, f is the frequency, i is an index which denotes motion regimes, i.e., SD ($i = 1$), DI ($i = 2$) and LTD ($i = 3$) frequency ranges, $T_1 = 2$ h (time period corresponding to the Nyquist frequency), $T_2 = 22$ h, $T_3 = 26$ h and $T_4 = 7$ days.

Appendix B

B1. Decomposition of the Root-Mean-Square Errors

[62] The analysis of the root-mean-square errors (RMSE) suffers from uncertainty both in space and time, otherwise

known as the "double-penalty" error [*Rife and Davis*, 2005]. In order to isolate the influence of phase errors in the biases of the mean and standard deviation, prior to the analysis of the model accuracy we decompose the RMSE [*Takacs*, 1985; *Murphy*, 1988] as follows:

$$\frac{1}{MN}\sum_{k=1}^{M}\sum_{i=1}^{N}\left(x_{i,k} - y_{i,k}\right)^2 = \frac{1}{M}\sum_{k=1}^{M}\left(\overline{x_k} - \overline{y_k}\right)^2 + \left[\sigma_k(x) - \sigma_k(y)\right]^2$$
$$+ 2\sigma_k(x)\sigma_k(y)[1 - r_k(x,y)] \tag{B1}$$

where x and y are the modeled and measured data, k and i are indices in space and time, M is the number of stations ($M = 4$), N is the number of elements of the time series ($N = 744$), σ is the standard deviation, r is the correlation coefficient between the modeled and measured data, and bars denote time-means. The three right-hand side terms of equation (B1) are the square of the bias of the mean, the square of the bias of the standard deviation and the square of the dispersion (phase) error, respectively.

References

Anthes, R. A., Y.-H. Kuo, E.-Y. Hsie, S. Low-Nam, and T. W. Bettge (1989), Estimation of skill and uncertainty in regional numerical models, *Q. J. R. Meteorol. Soc.*, 115, 763–806, doi:10.1002/qj.49711548803.

Belu, R., and D. Koracin (2009), Wind characteristics and wind energy potential in western Nevada, *Renewable Energy*, 34, 2246–2251, doi:10.1016/j.renene.2009.02.024.

Belušić, D., M. Žagar, and B. Grisogono (2007), Numerical simulation of pulsations in the bora wind, *Q. J. R. Meteorol. Soc.*, 133, 1371–1388, doi:10.1002/qj.129.

Cairns, M. M., and J. Corey (2003), Mesoscale model simulations of high-wind events in the complex terrain of western Nevada, *Weather Forecast.*, 18, 249–263, doi:10.1175/1520-0434(2003)018<0249:MMSOHE>2.0.CO;2.

Caldwell, P., H.-N. S. Chin, D. C. Bader, and G. Bala (2009), Evaluation of a WRF dynamical downscaling simulation over California, *Clim. Change*, 95, 499–521, doi:10.1007/s10584-009-9583-5.

Chen, F., and J. Dudhia (2001), Coupling an advanced land surface-hydrology model with the Penn State–NCAR MM5 Modeling System. Part II: Preliminary model validation, *Mon. Weather Rev.*, 129, 587–604, doi:10.1175/1520-0493(2001)129<0587:CAALSH>2.0.CO;2.

Chow, F. K., A. P. Weigel, R. L. Street, M. W. Rotach, and M. Xue (2006), High-resolution large-eddy simulations of flow in a steep alpine valley. Part I: Methodology, verification, and sensitivity experiments, *J. Appl. Meteorol. Climatol.*, 45, 63–86, doi:10.1175/JAM2322.1.

Colle, B. A., and C. F. Mass (1998), Windstorms along the western side of the Washington Cascade Mountains. Part I: A high-resolution observational and modeling study of the 12 February 1995 event, *Mon. Weather Rev.*, 126, 28–52, doi:10.1175/1520-0493(1998)126<0028:WATWSO>2.0.CO;2.

Conil, S., and A. Hall (2006), Local regimes of atmospheric variability: A case study of Southern California, *J. Clim.*, 19, 4308–4325, doi:10.1175/JCLI3837.1.

Cuxart, J., et al. (2006), Single-column model intercomparison for a stably stratified atmospheric boundary layer, *Boundary Layer Meteorol.*, 118, 273–303, doi:10.1007/s10546-005-3780-1.

Dudhia, J. (1989), Numerical study of convection observed during the winter monsoon experiment using a mesoscale two-dimensional model, *J. Atmos. Sci.*, 46, 3077–3107, doi:10.1175/1520-0469(1989)046<3077:NSOCOD>2.0.CO;2.

Ek, M. B., K. E. Mitchell, Y. Lin, E. Rogers, P. Grummann, V. Koren, G. Gayno, and J. D. Tarpley (2003), Implementation of Noah land surface model advances in the National Centers for Environmental Prediction

operational mesoscale Eta model, *J. Geophys. Res.*, *108*(D22), 8851, doi:10.1029/2002JD003296.

Feser, F. (2006), Enhanced detectability of added value in limited-area model results separated into different spatial scales, *Mon. Weather Rev.*, *134*, 2180–2190, doi:10.1175/MWR3183.1.

Giorgi, F. (2006), Regional climate modeling: Status and perspectives, *J. Phys. IV*, *139*, 101–118, doi:10.1051/jp4:2006139008.

Grell, G. A., J. Dudhia, and D. R. Stauffer (1994), A description of the fifth-generation Penn State/NCAR mesoscale mode (MM5), *Tech. Note NCAR/TN-398+STR*, 117 pp., Natl. Cent. for Atmos. Res., Boulder, Colo.

Grubišić, V., et al. (2008), The Terrain-Induced Rotor Experiment: A field campaign overview including observational highlights, *Bull. Am. Meteorol. Soc.*, *89*, 1513–1533, doi:10.1175/2008BAMS2487.1.

Hahmann, A. N., D. Rostkier-Edelstein, T. T. Warner, F. Vandenberghe, Y. Liu, R. Babarsky, and S. P. Swerdlin (2010), A reanalysis system for the generation of mesoscale climatographies, *J. Appl. Meteorol. Climatol.*, *49*, 954–972.

Horvath, K., A. Bajić, and S. Ivatek-Šahdan (2011), Dynamical downscaling of wind speed in complex terrain prone to bora-type flows, *J. Appl. Meteorol. Climatol.*, *50*, 1676–1691, doi:10.1175/2011JAMC2638.1.

Intergovernmental Panel on Climate Change (2007), *Climate Change 2007: The Physical Science Basis. Contribution of the Working Group I to the Fourth Assessment Report of the Intergovernmental Panel on Climate Change*, edited by S. Solomon et al., Cambridge Univ. Press, Cambridge, U. K.

Janjić, Z. I. (1996), The surface layer in the NCEP Eta model, paper presented at Eleventh Conference on Numerical Weather Prediction, Am. Meteorol. Soc., Norfolk, Va., 19–23 Aug.

Janjić, Z. I. (2001), Nonsingular implementation of the Mellor-Yamada level 2.5 scheme in the NCEP Meso model, *Off. Note 437*, 61 pp., Natl. Cent. for Environ. Prot., Boulder, Colo.

Jeglum, M. E., W. J. Steenburgh, T. P. Lee, and L. F. Bosart (2010), Multi-reanalysis climatology of intermountain cyclones, *Mon. Weather Rev.*, *138*, 4035–4053, doi:10.1175/2010MWR3432.1.

Jiménez, P. A., J. F. Gonzálaz-Rouco, E. García-Bustamente, J. Navarro, J. P. Montávez, J. Vilá-Guerau de Arellano, J. Dudhia, and A. Munoz-Roldan (2010), Surface wind regionalization over complex terrain: Evaluation and analysis of a high-resolution WRF simulation, *J. Appl. Meteorol. Climatol.*, *49*, 268–287, doi:10.1175/2009JAMC2175.1.

Kain, J. S. (2004), The Kain-Fritsch convective parameterization: An update, *J. Appl. Meteorol.*, *43*, 170–181, doi:10.1175/1520-0450(2004)043<0170:TKCPAU>2.0.CO;2.

Kain, J. S., and J. M. Fritsch (1993), Convective parameterization for mesoscale models: The Kain-Fritsch scheme, in *The Representation of Cumulus Convection in Numerical Models*, edited by K. A. Emanuel and D. J. Raymond, pp. 165–170, Am. Meteorol. Soc., Boston, Mass.

Koracin, D., and C. E. Dorman (2001), Marine atmospheric boundary layer divergence and clouds along California in June 1996, *Mon. Weather Rev.*, *129*, 2040–2056, doi:10.1175/1520-0493(2001)129<2040:MABLDA>2.0.CO;2.

Laprise, R. (1992), The Euler equations of motion with hydrostatic pressure as an independent variable, *Mon. Weather Rev.*, *120*, 197–207, doi:10.1175/1520-0493(1992)120<0197:TEEOMW>2.0.CO;2.

Leung, L. R., Y. H. Kuo, and J. Tribbia (2006), Research needs and directions of regional climate modeling using WRF and CCSM, *Bull. Am. Meteorol. Soc.*, *87*, 1747–1751, doi:10.1175/BAMS-87-12-1747.

Lo, J. C.-F., Z.-L. Yang, and R. A. Pielke Sr. (2008), Assessment of three dynamical climate downscaling methods using the Weather Research and Forecasting (WRF) model, *J. Geophys. Res.*, *113*, D09112, doi:10.1029/2007JD009216.

Mass, C. F., D. Ovens, K. Westrick, and B. A. Colle (2002), Does increasing horizontal resolution produce more skillful forecast?, *Bull. Am. Meteorol. Soc.*, *83*, 407–430, doi:10.1175/1520-0477(2002)083<0407:DIHRPM>2.3.CO;2.

Mellor, G. L., and T. Yamada (1974), A hierarchy of turbulence closure models for planetary boundary layers, *J. Atmos. Sci.*, *31*, 1791–1806, doi:10.1175/1520-0469(1974)031<1791:AHOTCM>2.0.CO;2.

Mellor, G. L., and T. Yamada (1982), Development of a turbulence closure model for geophysical fluid problems, *Rev. Geophys.*, *20*, 851–875, doi:10.1029/RG020i004p00851.

Mesinger, F., et al. (2006), North American regional reanalysis, *Bull. Am. Meteorol. Soc.*, *87*, 343–360, doi:10.1175/BAMS-87-3-343.

Mlawer, E. J., S. J. Taubman, P. D. Brown, M. J. Iacono, and S. A. Clough (1997), Radiative transfer for inhomogeneous atmosphere: RRTM, a validated correlated-k model for the longwave, *J. Geophys. Res.*, *102*(D14), 16,663–16,682, doi:10.1029/97JD00237.

Murphy, A. H. (1988), Skill scores based on the mean square error and their relationships to the correlation coefficient, *Mon. Weather Rev.*, *116*, 2417–2424, doi:10.1175/1520-0493(1988)116<2417:SSBOTM>2.0.CO;2.

Pan, Z., E. Takle, W. Gutowski, and R. Turner (1999), Long simulation of regional climate as a sequence of short segments, *Mon. Weather Rev.*, *127*, 308–321, doi:10.1175/1520-0493(1999)127<0308:LSORCA>2.0.CO;2.

Qian, J.-H., A. Seth, and S. Zebiak (2003), Reinitialized versus continuous simulations for regional climate downscaling, *Mon. Weather. Rev.*, *131*, 2857–2874, doi:10.1175/1520-0493(2003)131<2857:RVCSFR>2.0.CO;2.

Reisner, J., R. M. Rasmussen, and R. T. Bruintjes (1998), Explicit forecasting of supercooled liquid water in winter storms using the MM5 forecast model, *Q. J. R. Meteorol. Soc.*, *124*, 1071–1107, doi:10.1002/qj.49712454804.

Rife, D. L., and C. A. Davis (2005), Verification of temporal variations in mesoscale numerical wind forecasts, *Mon. Weather Rev.*, *133*, 3368–3381, doi:10.1175/MWR3052.1.

Rife, D. L., C. A. Davis, and Y. Liu (2004), Predictability of low-level winds by mesoscale meteorological models, *Mon. Weather Rev.*, *132*, 2553–2569, doi:10.1175/MWR2801.1.

Rife, D. L., J. O. Pinto, A. J. Monaghan, C. A. Davis, and J. R. Hannan (2010), Global distribution and characteristics of diurnally varying low-level jets, *J. Clim.*, *23*, 5041–5064, doi:10.1175/2010JCLI3514.1.

Rockel, B., C. L. Castro, R. A. Pielke Sr., H. von Storch, and G. Leoncini (2008), Dynamical downscaling: Assessment of model system dependent retained and added variability for two different regional climate models, *J. Geophys. Res.*, *113*, D21107, doi:10.1029/2007JD009461.

Skamarock, W. C., J. B. Klemp, J. Dudhia, D. O. Gill, D. M. Barker, M. G. Duda, X.-Y. Huang, W. Wang, and J. G. Powers (2008), Description of the Advanced Research WRF version 4, *Rep. NCAR/TN-475++STR*, Natl. Cent. for Atmos. Res., Boulder, Colo.

Stewart, J. Q., C. D. Whiteman, W. J. Steenburgh, and X. Bian (2002), A climatological study of thermally driven wind systems if the U.S. intermountain west, *Bull. Am. Meteorol. Soc.*, *83*, 699–708, doi:10.1175/1520-0477(2002)083<0699:ACSOTD>2.3.CO;2.

Storm, B., J. Dudhia, S. Basu, A. Swift, and I. Giammanco (2009), Evaluation of the Weather Research and Forecasting model on forecasting low-level jets: Implications for wind energy, *Wind Energy*, *12*, 81–90, doi:10.1002/we.288.

Takacs, L. L. (1985), A two-step scheme for the advection equation with minimized dissipation and dispersion errors, *Mon. Weather Rev.*, *113*, 1050–1065, doi:10.1175/1520-0493(1985)113<1050:ATSSFT>2.0.CO;2.

Thompson, G., R. M. Rasmussen, and K. Manning (2004), Explicit forecasts of winter precipitation using an improved bulk microphysics scheme. Part I: Description and sensitivity analysis, *Mon. Weather Rev.*, *132*, 519–542, doi:10.1175/1520-0493(2004)132<0519:EFOWPU>2.0.CO;2.

Trapp, R. J., E. D. Robinson, M. E. Baldwin, N. S. Diffenbaugh, and B. R. J. Schwedler (2011), Regional climate of hazardous convective weather through high-resolution dynamical downscaling, *Clim. Dyn.*, *37*, 677–688, doi:10.1007/s00382-010-0826-y.

von Storch, H., H. Langenberg, and F. Feser (2000), A spectral nudging technique for dynamical downscaling purposes, *Mon. Weather Rev.*, *128*, 3664–3673, doi:10.1175/1520-0493(2000)128<3664:ASNTFD>2.0.CO;2.

Warner, T. T., R. A. Peterson, and R. E. Treadon (1997), A tutorial on lateral boundary conditions as a basic and potentially serious limitation to regional numerical weather prediction, *Bull. Am. Meteorol. Soc.*, *78*, 2599–2617, doi:10.1175/1520-0477(1997)078<2599:ATOLBC>2.0.CO;2.

Welch, P. D. (1967), The use of fast Fourier transform for the estimation of power spectra: A method based on time averaging over short, modified periodograms, *IEEE Trans. Audio Electroacoust.*, *15*(2), 70–73, doi:10.1109/TAU.1967.1161901.

Whiteman, C. D. (2000), *Mountain Meteorology: Fundamentals and Applications*, Oxford Univ. Press, New York.

Wyngaard, J. C. (2004), Toward numerical modeling in the "terra incognita," *J. Atmos. Sci.*, *61*, 1816–1826, doi:10.1175/1520-0469(2004)061<1816:TNMITT>2.0.CO;2.

Žagar, N., M. Žagar, J. Cedilnik, G. Gregorič, and J. Rakovec (2006), Validation of mesoscale low-level winds obtained by dynamical downscaling of ERA-40 over complex terrain, *Tellus, Ser. A*, *58*, 445–455.

Zängl, G., B. Chimani, and C. Häberli (2004), Numerical simulations of the foehn in the Rhine valley on 24 October 1999 (MAP IOP 10), *Mon. Weather Rev.*, *132*, 368–389, doi:10.1175/1520-0493(2004)132<0368:NSOTFI>2.0.CO;2.